Acta Oceanol. Sin., 2014, Vol. 33, No. 3, P. 58–81
DOI: 10.1007/s13131-014-0412-y
http://www.hyxb.org.cn
E-mail: hyxbe@263.net

Energetics of lateral eddy diffusion/advection: Part IV. Energetics of diffusion/advection in sigma coordinates and other coordinates

HUANG Rui Xin[1]*

[1] Department of Physical Oceanography, Woods Hole Oceanographic Institution, MA 02543-1050, USA

Received 30 August 2013; accepted 17 December 2013

The Chinese Society of Oceanography and Springer-Verlag Berlin Heidelberg 2014

Abstract

Gravitational potential energy (GPE) source and sink due to stirring and cabbeling associated with sigma diffusion/advection is analyzed. It is shown that GPE source and sink is too big, and they are not closely linked to physical property distribution, such as temperature, salinity and velocity. Although the most frequently quoted advantage of sigma coordinate models are their capability of dealing with topography; the excessive amount of GPE source and sink due to stirring and cabbeling associated with sigma diffusion/advection diagnosed from our analysis raises a very serious question whether the way lateral diffusion/advection simulated in the sigma coordinates model is physically acceptable. GPE source and sink in three coordinates is dramatically different in their magnitude and patterns. Overall, in terms of simulating lateral eddy diffusion and advection isopycnal coordinates is the best choice and sigma coordinates is the worst. The physical reason of the excessive GPE source and sink in sigma coordinates is further explored in details. However, even in the isopycnal coordinates, simulation based on the Eulerian coordinates can be contaminated by the numerical errors associated with the advection terms.

Key words: energetics of horizontal advection, energetics of horizontal eddy diffusion, energetics of isopycnal advection, energetics of isopycnal eddy diffusion, energetics of sigma advection diffusion, energetics of sigma eddy diffusion

Citation: Huang Rui Xin. 2014. Energetics of lateral eddy diffusion/advection: Part IV. Energetics of diffusion/advection in sigma coordinates and other coordinates. Acta Oceanologica Sinica, 33(3): 58–81, doi: 10.1007/s13131-014-0412-y

1 Introduction

Sigma coordinates has been widely used in both atmospheric and oceanic models. In oceanography, sigma coordinate (or the so-called *s*-coordinate) has been widely used. Although most applications are targeted for coastal regime, such models have been used for basin-scale circulation as well. One of the well known problems in sigma coordinate models is the lateral pressure gradient error associated with steep topography. Many studies have been carried out to overcome this problem, including using different finite difference schemes or even smoothing topography.

All such approaches are based on some mathematical techniques, and the results thus obtained are difficult to be compared with results from other approaches or models based on different coordinates. Thus, we postulate using gravitational potential energy (GPE, hereafter) source and sink due to stirring and cabbeling associated with lateral diffusion/advection as the criterion for evaluate the model's performance.

This part of this study is organized as follows. In Section 2.1, we formulate the GPE source and sink due to stirring/cabbeling associated with sigma diffusion/advection. In Section 2.2, these formulae are used to calculate the GPE source and sink in the world oceans, based on the SODA data (Carton and Giese, 2008). As will be shown, GPE source and sink in sigma coordinates is huge, and we will explore the reason for such a problem in Section 2.3. In particular, an idealized dataset will be constructed in which there is no horizontal temperature and salinity gradient. Simple calculations show that even in such an idealized ocean, sigma diffusion/advection can still generate a large amount of GPE source and sink. The potential problem of handling topography in sigma coordinates is further examined from the physical point of view in the Appendix.

The results obtained from three coordinates: horizontal, isopycnal and sigma coordinates, are compared in Section 3. In particular, the large numerical diffusivity associated with the sigma coordinates is further examined, and such problems may be intrinsic to the fundamental formulation of this coordinates system. We conclude this study in Section 4.

2 Energetics of sigma diffusion/advection

2.1 *GPE change due to sigma diffusion and advection*

2.1.1 *GPE change due to stirring associated with sigma diffusion*

During stirring in sigma coordinates parcels move to different pressure levels, so that potential density based on the pressure at the center of this grid box should be used. In addition, the cross-boundary tracer transport due to stirring is proportional to the height of the inter-box boundary. The equation corresponding to Eq. (4) in Part III (Huang, 2014c) is as follows

*Corresponding author, E-mail: rhuang@whoi.edu

$$\Delta h_{i,j,k}\Delta x_j\Delta y\frac{\partial\rho_{i,j,k}}{\partial t}=K\times$$
$$\left[\frac{\Delta h_{i+1/2,j,k}\Delta y}{\Delta x_j}\left(\sigma_{i+1,j,k}-\rho_{i,j,k}\right)+\frac{\Delta h_{i-1/2,j,k}\Delta y}{\Delta x_j}\left(\sigma_{i-1,j,k}-\rho_{i,j,k}\right)+\right.$$
$$\left.\frac{\Delta h_{i,j+1/2,k}\Delta x_{j+1/2}}{\Delta y}\left(\sigma_{i,j+1,k}-\rho_{i,j,k}\right)+\frac{\Delta h_{i,j-1/2,k}\Delta x_{j-1/2}}{\Delta y}\left(\sigma_{i,j-1,k}-\rho_{i,j,k}\right)\right],\quad(1)$$

where $\Delta h_{i,j,k}$ is the thickness of grid box, $\Delta h_{i+1/2,j,k}$ is the thickness of the right-side boundary, σ denotes potential density using pressure $p_{i,j,k}$ at the center of grid point(i, j, k) as the reference pressure. For example, $\sigma_{i+1,j,k}=\sigma(S_{i+1,j,k}, \Theta_{i+1,j,k}, p_{i,j,k})$ is the potential density for the water parcel in grid box (i+1, j, k), and it is also the *in-situ* density for this water parcel when it arrives at grid point (i, j, k); $\Theta=\Theta(S_{i+1,j,k}, T_{i+1,j,k}, p_{i+1,j,k}, p_{i,j,k})$ is the potential temperature of the water parcel in grid box (i+1, j, k), using $p_{i,j,k}$ as the reference pressure.

Thus, the corresponding rate of GPE change due to stirring associated with sigma diffusion is

$$\dot{\chi}_{\rm stir}^{\rm sigma,diffu}=CKp_{i,j,k}\times$$
$$\left[\frac{\Delta h_{i+1/2,j,k}\Delta y}{\Delta x_j}\left(1-\frac{\sigma_{i+1,j,k}}{\rho_{i,j,k}}\right)+\frac{\Delta h_{i-1/2,j,k}\Delta y}{\Delta x_j}\left(1-\frac{\sigma_{i-1,j,k}}{\rho_{i,j,k}}\right)+\right.$$
$$\left.\frac{\Delta h_{i,j+1/2,k}\Delta x_{j+1/2}}{\Delta y}\left(1-\frac{\sigma_{i,j+1,k}}{\rho_{i,j,k}}\right)+\frac{\Delta h_{i,j-1/2,k}\Delta x_{j-1/2}}{\Delta y}\left(1-\frac{\sigma_{i,j-1,k}}{\rho_{i,j,k}}\right)\right],\quad(2)$$

where C=10 000 is a unit conversion factor, if pressure in 10^4 Pa is used. For a square grid and with no topography, Eq. (2) is reduced to the same expression as Eq. (8) in Part III (Huang, 2014c).

$$\dot{\chi}_{\rm stir}^{\rm hori,diffu}=CKp_k\Delta h_{i,j,k}\left[4-\left(\rho_{i+1,j,k}+\rho_{i-1,j,k}+\rho_{i,j+1,k}+\rho_{i,j-1,k}\right)/\rho_{i,j,k}\right].(2')$$

Therefore, if the density is a local minimum, lateral water mass exchanging before subscale diffusion release the mean state GPE, i.e. it is a sink of GPE. On the other hand, if density is a local maximum, lateral stirring gives rise to increase of the mean state GPE.

However, the sea floor is not flat and sigma surfaces dramatically deviate from pressure surfaces. As a result, sigma stirring may be quite different from that of horizontal stirring discussed in Part III (Huang, 2014c). In fact, during sigma stirring water parcels from quite different depths can be brought together to refresh the water properties at a given grid box. Such a parameterization means refreshing of the original water masses by a combination of dramatically different water masses. As a result, the GPE of the system can change greatly.

2.1.2 *GPE change due to cabbeling associated with sigma diffusion*

We denote water properties from the right, left, north, and south by subscript *r*, *l*, *n* and *s*.

For example, subscale diffusion between water parcel in a grid point and water parcel on the sigma surface at its right-hand side involves potential temperature $\Theta_0=T_0$ and $\Theta_r=\Theta(S_r, T_r, p_r, S_r, P_{i,j,k})$, where S_r, T_r and p_r are the corresponding temperature, salinity and pressure in the right-hand side grid box.

As discussed in Section 2, Eq. (9) of Part III (Huang, 2014c), over a time interval of Δt, the temperature perturbation at this grid point is

$$\Delta T_{i,j,k}=B\left[\frac{\Delta h_{i+1/2,j,k}\Delta y}{\Delta x_j}\left(\Theta_r-T_0\right)+\frac{\Delta h_{i-1/2,j,k}\Delta y}{\Delta x_j}\left(\Theta_l-T_0\right)+\right.$$
$$\left.\frac{\Delta h_{i,j+1/2,k}\Delta x_{j+1/2}}{\Delta y}\left(\Theta_n-T_0\right)+\frac{\Delta h_{i,j-1/2,k}\Delta x_{j-1/2}}{\Delta y}\left(\Theta_s-T_0\right)\right],\quad(3)$$
$$B=\frac{K\Delta t}{\Delta x_j\Delta y\Delta h_{i,j,k}}.$$

After a time interval of

$$\Delta t=\frac{\Delta x_j\Delta y\Delta h_{i,j,k}}{KD_{i,j,k}},$$
$$D_{i,j,k}=\frac{\Delta y}{\Delta x_j}\Delta h_{i+1/2,j,k}+\frac{\Delta y}{\Delta x_j}\Delta h_{i-1/2,j,k}+\quad(4)$$
$$\frac{\Delta x_{j+1/2}}{\Delta y}\Delta h_{i,j+1/2,k}+\frac{\Delta x_{j-1/2}}{\Delta y}\Delta h_{i,j-1/2,k},$$

the new mean potential temperature, salinity and density at this grid point are

$$\overline{T}_{i,j,k}=T_{i,j,k}+\Delta T_{i,j,k}$$
$$=\left[\frac{\Delta y}{\Delta x_j}\Delta h_{i+1/2,j,k}\Theta_r+\frac{\Delta y}{\Delta x_j}\Delta h_{i-1/2,j,k}\Theta_l+\right.$$
$$\left.\frac{\Delta x_{j+1/2}}{\Delta y}\Delta h_{i,j+1/2,k}\Theta_n+\frac{\Delta x_{j-1/2}}{\Delta y}\Delta h_{i,j-1/2,k}\Theta_s\right]D_{i,j,k}^{-1},\quad(5)$$

$$\overline{S}_{i,j,k}=\left[\frac{\Delta y}{\Delta x_j}\Delta h_{i+1/2,j,k}S_r+\frac{\Delta y}{\Delta x_j}\Delta h_{i-1/2,j,k}S_l+\right.$$
$$\left.\frac{\Delta x_{j+1/2}}{\Delta y}\Delta h_{i,j+1/2,k}S_n+\frac{\Delta x_{j-1/2}}{\Delta y}\Delta h_{i,j-1/2,k}S_s\right]D_{i,j,k}^{-1},\quad(6)$$

$$\overline{\rho}_{i,j,k}=\left[\frac{\Delta y}{\Delta x_j}\Delta h_{i+1/2,j,k}\rho_r+\frac{\Delta y}{\Delta x_j}\Delta h_{i-1/2,j,k}\rho_l+\right.$$
$$\left.\frac{\Delta x_{j+1/2}}{\Delta y}\Delta h_{i,j+1/2,k}\rho_n+\frac{\Delta x_{j-1/2}}{\Delta y}\Delta h_{i,j-1/2,k}\rho_s\right]D_{i,j,k}^{-1}.\quad(7)$$

After subscale diffusion of water parcels in this grid box, the new density is

$$\rho_{i,j,k,\rm mix}=\rho\left(\overline{S}_{i,j,k},\overline{T}_{i,j,k},p_{i,j,k}\right).\quad(8)$$

The total change of GPE of the water column above this water parcel is

$$\Delta\chi_{\rm cabb}^{\rm sigma,diffu}=p_{i,j,k}\delta\Delta h_{i,j,k}\Delta x_j\Delta y$$
$$=p_{i,j,k}\left(\overline{\rho}_{i,j,k}/\rho_{i,j,k,\rm mix}-1\right)\Delta h_{i,j,k}\Delta x_j\Delta y.\quad(9)$$

Thus, over the time period of Δt the mean rate of GPE change is

$$\dot{\chi}_{\rm cabb}^{\rm sigma,diffu}=Cp_{i,j,k}\left(\overline{\rho}_{i,j,k}/\rho_{i,j,k,\rm mix}-1\right)\Delta h_{i,j,k}\Delta x_j\Delta y/\Delta t$$
$$=CKp_{i,j,k}\left(\overline{\rho}_{i,j,k}/\rho_{i,j,k,\rm mix}-1\right)D_{i,j,k}.\quad(10)$$

2.1.3 *GPE releasing due to stirring associated with sigma advection*

We now turn to the contribution associated with the lateral advection in the sigma coordinates. For simplicity, in the tracer balance equation we retain the advection terms only and omit other terms

$$\frac{\partial C}{\partial t} = -\nabla_\sigma \cdot \left(\vec{U}_\sigma C\right), \tag{11}$$

where the subscript "σ" indicates the lateral operator and lateral velocity component in the sigma coordinates. Our study here is focused on GPE change due to lateral advection on scales of 1 to 100 km. For such large horizontal scales, we will ignore the difference in salt and temperature diffusion. The zonal and meridional coordinates is denoted as(x, y); thus, $\Delta x=r\cos\theta\Delta\lambda$, $\Delta y=r\Delta\theta$, where r is the radius of the Earth and λ and θ are the longitude and latitude. The time change rate of density is due to advection from left, right, south and north of the give grid box; thus, for the density balance, Eq. (11) can be converted into the following form

$$\Delta h_{i,j,k}\Delta x_j \Delta y \frac{\partial \rho_{i,j,k}}{\partial t} = \Big[\Delta y\left(\Delta hU\rho\right)^- - \Delta y\left(\Delta hU\rho\right)^+ + \left(\Delta x\Delta hV\rho\right)^- - \left(\Delta x\Delta hV\rho\right)^+\Big]. \tag{12}$$

Note that in a sigma coordinates, parcels move to different pressure levels, so that potential density based on the pressure at the center of this grid box should be used. In addition, the cross-boundary tracer transport due to stirring is proportional to the height of the inter-box boundary.

Density change in a grid box $\delta\rho_{i,j,k}$ gives rise to thickness change

$$\delta h_{i,j,k} = -\Delta h_{i,j,k}\delta\rho_{i,j,k} / \overline{\rho}, \tag{13}$$

where $\Delta h_{i',j',k}$ is the thickness of the grid box. Assuming the water parcel has a horizontal areaA_S, and the *in-situ* pressure is p_k, the increment of the total GPE of the water column above is

$$\delta\chi = p_k A_S \delta h_{i,j,k} = -p_k A_S \Delta h_{i,j,k}\delta\rho_{i,j,k} / \overline{\rho}. \tag{14}$$

Using Eq. (12), the rate of GPE change due to stirring associated with horizontal advection is

$$\dot{\chi}_{\text{stir}}^{\text{sigma,advec}} = Cp_k\Big[\Delta y\left(\Delta hU\rho\right)^- - \Delta y\left(\Delta hU\rho\right)^+ + \left(\Delta x\Delta hV\rho\right)^- - \left(\Delta x\Delta hV\rho\right)^+\Big] / \overline{\rho}, \tag{15}$$

where C=10 000 is a unit conversion factor, if pressure in unit of (10^4 Pa) is used.

In many numerical models the central difference scheme is commonly used in the tracer transport equation; thus, the flux is calculated as follows:

$$\begin{aligned}
\left(\Delta x\Delta hV\rho\right)^- &= \frac{\Delta x_{j-1/2}}{8}\left(\Delta h_{i,j-1,k}+\Delta h_{i,j,k}\right)\left(V_{i,j-1,k}+V_{i,j,k}\right)\left(\sigma_{i,j-1,k}+\rho_{i,j,k}\right),\\
\left(\Delta x\Delta hV\rho\right)^+ &= \frac{\Delta x_{j+1/2}}{8}\left(\Delta h_{i,j+1,k}+\Delta h_{i,j,k}\right)\left(V_{i,j+1,k}+V_{i,j,k}\right)\left(\sigma_{i,j+1,k}+\rho_{i,j,k}\right),\\
\Delta y\left(\Delta hU\rho\right)^- &= \frac{\Delta y}{8}\left(\Delta h_{i-1,j,k}+\Delta h_{i,j,k}\right)\left(U_{i-1,j,k}+U_{i,j,k}\right)\left(\sigma_{i-1,j,k}+\rho_{i,j,k}\right),\\
\Delta y\left(\Delta hU\rho\right)^+ &= \frac{\Delta y}{8}\left(\Delta h_{i+1,j,k}+\Delta h_{i,j,k}\right)\left(V_{i+1,j,k}+V_{i,j,k}\right)\left(\sigma_{i+1,j,k}+\rho_{i,j,k}\right).
\end{aligned} \tag{16}$$

This formulation includes the contribution due to the vertical upwelling associated with the horizontal divergence. Since GPE change associated with the vertical motions is not the focus in this study, we will be concentrated on the contribution due to the non-divergent component of the horizontal velocity field. Thus, we need to subtract the upwelling and downwelling due to the horizontal convergence, which contribution is

$$\Big[\Delta y\left(\Delta hU\right)^- - \Delta y\left(\Delta hU\right)^+ + \left(\Delta x\Delta hV\right)^- - \left(\Delta x\Delta hV\right)^+\Big]\rho_{i,j,k}. \tag{17}$$

Finally, the corresponding GPE change is

$$\begin{aligned}
\dot{\chi}_{\text{stir}}^{\text{sigma,advec}} = &\frac{Cp_k}{8\rho_{i,j,k}}\times\\
&\Big[\Delta y\left(\Delta h_{i-1,j,k}+\Delta h_{i,j,k}\right)\left(U_{i-1,j,k}+U_{i,j,k}\right)\left(\sigma_{i-1,j,k}-\rho_{i,j,k}\right)-\\
&\Delta y\left(\Delta h_{i+1,j,k}+\Delta h_{i,j,k}\right)\left(U_{i+1,j,k}+U_{i,j,k}\right)\left(\sigma_{i+1,j,k}-\rho_{i,j,k}\right)+\\
&\Delta x_{j-1/2}\left(\Delta h_{i,j-1,k}+\Delta h_{i,j,k}\right)\left(V_{i,j-1,k}+V_{i,j,k}\right)\left(\sigma_{i,j-1,k}-\rho_{i,j,k}\right)-\\
&\Delta x_{j+1/2}\left(\Delta h_{i,j+1,k}+\Delta h_{i,j,k}\right)\left(U_{i,j+1,k}+U_{i,j,k}\right)\left(\sigma_{i,j1,k}-\rho_{i,j,k}\right)\Big].
\end{aligned} \tag{18}$$

2.1.4 *GPE change due to cabbeling associated with sigma advection*

Similar to the discussion in the previous section, change of GPE due to cabbeling associated with advection in sigma coordinates can be derived. The corresponding temperature change is now in the following form

$$\begin{aligned}
\Delta T_{i,j,k} = &\frac{\Delta t}{8\Delta x_j\Delta y\Delta h_{i,j,k}}\times\\
&\Big[\Delta y\left(\Delta h_{i-1,j,k}+\Delta h_{i,j,k}\right)\left(U_{i-1,j,k}+U_{i,j,k}\right)\left(\Theta_{i-1,j,k}-T_{i,j,k}\right)-\\
&\Delta y\left(\Delta h_{i+1,j,k}+\Delta h_{i,j,k}\right)\left(U_{i+1,j,k}+U_{i,j,k}\right)\left(\Theta_{i+1,j,k}-T_{i,j,k}\right)+\\
&\Delta x_{j-1/2}\left(\Delta h_{i,j-1,k}+\Delta h_{i,j,k}\right)\left(V_{i,j-1,k}+V_{i,j,k}\right)\left(\Theta_{i,j-1,k}-T_{i,j,k}\right)-\\
&\Delta x_{j+1/2}\left(\Delta h_{i,j+1,k}+\Delta h_{i,j,k}\right)\left(V_{i,j+1,k}+V_{i,j,k}\right)\left(\Theta_{i,j+1,k}-T_{i,j,k}\right)\Big]\\
= &\frac{\Delta t}{8\Delta h_{i,j,k}}\times\\
&\Big[c_1 sign(U_{i-1,j,k}+U_{i,j,k})\left(\Theta_{i-1,j,k}-T_{i,j,k}\right)-\\
&c_2 sign(U_{i+1,j,k}+U_{i,j,k})\left(\Theta_{i+1,j,k}-T_{i,j,k}\right)+\\
&c_3 sign(V_{i,j-1,k}+V_{i,j,k})\left(\Theta_{i,j-1,k}-T_{i,j,k}\right)-\\
&c_4 sign(V_{i,j+1,k}+V_{i,j,k})\left(\Theta_{i,j+1,k}-T_{i,j,k}\right)\Big],
\end{aligned} \tag{19}$$

$$c_1 = \frac{1}{\Delta x_j}\left|U_{i-1,j,k} + U_{i,j,k}\right|\left(\Delta h_{i-1,j,k} + \Delta h_{i,j,k}\right),$$

$$c_2 = \frac{1}{\Delta x_j}\left|U_{i+1,j,k} + U_{i,j,k}\right|\left(\Delta h_{i+1,j,k} + \Delta h_{i,j,k}\right),$$

$$c_3 = \frac{\Delta x_{j-1/2}}{\Delta x_j \Delta y}\left|V_{i,j-1,k} + V_{i,j,k}\right|\left(\Delta h_{i,j-1,k} + \Delta h_{i,j,k}\right),$$

$$c_4 = \frac{\Delta x_{j+1/2}}{\Delta x_j \Delta y}\left|V_{i,j+1,k} + V_{i,j,k}\right|\left(\Delta h_{i,j+1,k} + \Delta h_{i,j,k}\right),$$

where $\Theta_{i-1,j,k}$ is the potential temperature for water parcel coming from grid point (i–1, j, k), using pressure at grid point (i, j, k) as the reference pressure, and terms with other subscripts are defined similarly. If we select the time interval as

$$\Delta t = 1/C_j,\ C_j = \Delta h_{i,j,k}\left(c_1 + c_2 + c_3 + c_4\right). \tag{20}$$

Then Eq. (19) is reduced to

$$\begin{aligned}\Delta T_{i,j,k} = \frac{1}{4C_j}\Big[&c_1 sign(U_{i-1,j,k} + U_{i,j,k})\left(\Theta_{i-1,j,k} - T_{i,j,k}\right) - \\ &c_2 sign(U_{i+1,j,k} + U_{i,j,k})\left(\Theta_{i+1,j,k} - T_{i,j,k}\right) + \\ &c_3 sign(V_{i,j-1,k} + V_{i,j,k})\left(\Theta_{i,j-1,k} - T_{i,j,k}\right) - \\ &c_4 sign(V_{i,j+1,k} + V_{i,j,k})\left(\Theta_{i,j+1,k} - T_{i,j,k}\right)\Big].\end{aligned} \tag{21}$$

Therefore, the temperature perturbation is the weighted mean of the normalized transport of temperature anomaly through all side boundaries. The new temperature at the end of this time interval is

$$\overline{T}_{i,j,k} = T_{i,j,k} + \Delta T_{i,j,k}\ . \tag{22}$$

Similarly, the new salinity and density (before mixing) are

$$\overline{S}_{i,j,k} = S_{i,j,k} + \Delta S_{i,j,k},\ \overline{\rho}_{i,j,k} = \rho_{i,j,k} + \Delta\rho_{i,j,k}\ . \tag{23}$$

In the density calculation, the potential density should be used in the formula corresponding to Eq. (21). The final value of density at this grid is

$$\rho_{i,j,k,\mathrm{mix}} = \rho\left(\overline{S}_{i,j,k}, \overline{T}_{i,j,k}, p_k\right). \tag{24}$$

The change in GPE of water column above the center of this grid box is

$$\Delta\chi_{\mathrm{cabb}}^{\mathrm{sigma,advec}} = p_k \delta\Delta h_{i,j,k}\Delta x_j \Delta y = p_k\left(\overline{\rho}_{i,j,k}/\rho_{i,j,k,\mathrm{mix}} - 1\right)\Delta h_{i,j,k}\Delta x_j \Delta y\ . \tag{25}$$

Thus, over the time period of Δt the mean strength of GPE sink due to cabbeling associated with horizontal advection is

$$\begin{aligned}\dot{\chi}_{\mathrm{cabb}}^{\mathrm{sigma,advec}} &= p_k\left(\overline{\rho}_{i,j,k}/\rho_{i,j,k,\mathrm{mix}} - 1\right)\Delta h_{i,j,k}\Delta x_j \Delta y/\Delta t \\ &= C p_k\left(\overline{\rho}_{i,j,k}/\rho_{i,j,k,\mathrm{mix}} - 1\right)C_j \Delta h_{i,j,k}\Delta x_j \Delta y\ .\end{aligned} \tag{26}$$

2.2 *Apply to the world oceans*

First of all, in order to calculate the GPE balance in the world oceans based on the sigma coordinates, we need to create the corresponding data. The 50-year mean SODA data (Carton and Giese, 2008) has 40 layers in the vertical direction, with the center of grid at: 5.01, 15.07, 25.28, 35.76, 46.61, 57.98, 70.02, 82.92, 96.92, 112.32, 129.49, 148.96, 171.4, 197.79, 229.48, 268.46, 317.65, 381.39, 465.91, 579.31, 729.35, 918.37, 1 139.15, 1 378.57, 1 625.7, 1 875.11, 2 125.01, 2 375, 2 625, 2 875, 3 125, 3 375, 3 625, 3 875, 4 125, 4 375, 4 625, 4 875, 5 125, 5 375 m. Assuming the boundary between each pair of grid is half way between the centers, the upper and lower boundaries of each grid is obtained. In addition, the ratio of depth at these standard grid points and the deepest grid point gives rise to the ratio of sigma coordinates for each station in the world oceans.

Using the depth of the water column at each station, one can construct the corresponding sigma grid at this station. The corresponding temperature, salinity and horizontal velocity at this station taken from SODA data can be interpolated to generate the corresponding temperature, salinity and horizontal velocity at the sigma grid for this station. Note that lateral velocity is slightly different from the horizontal velocity at each sigma grid. In general, however, the aspect ratio of the sigma grid is so small, and even for the steepest topography it is no more than 1/100. Therefore, we will take the horizontal velocity interpolated from the SODA data as the lateral velocity in the sigma coordinates. In this way, two sets of data in sigma coordinates were generated, with horizontal resolution of 1° and 0.5°. Note that the lateral diffusivity is set to 1 000 m^2/s for the case of 1° resolution and 500 m^2/s for the case of 0.5° resolution.

Using the SODA data, the GPE source and sink due to stirring and cabbeling associated with sigma diffusion and advection is shown in the following Table 1.

In general, the GPE source and sink calculated in the sigma coordinates is much larger than those in the z-coordinates and the isopycnal coordinates. For the case with 1° resolution, the source and sink due to stirring associated with diffusion is 123.8 and 48.9 TW, with a net contribution of 74.9 TW. The sink due to diffusion associated with cabbeling is 16 TW. The huge terms of

Table 1. GPE source and sink (TW) in sigma coordinates

Terms	Grid resolution	Stirring			Cabbeling		
		Source	Sink	Net	Source	Sink	Net
Diffusion	1.0	123.8	−48.9	74.9	0	−16.0	−16.0
	0.5	129.2	−67.6	61.6	0	−13.1	−13.1
Advection	1.0	13.4	−13.3	0.16	0.78	−0.55	0.23
	0.5	21.9	−22.2	−0.30	1.23	−0.98	0.25

GPE source and sink indicate that the parameterization of lateral diffusion in terms of along sigma surface may be unphysical.

The GPE source and sink due to stirring associated with sigma advection is 13.4 and 13.3 TW, respectively. These terms are quite large. For the case with 1° resolution, the GPE source and sink due to cabbeling associated with sigma advection is 0.78 and 0.55 TW. These are much larger than the corresponding terms in isopycnal coordinates and z-coordinates. In particular, a positive GPE source of 0.78 TW is a large artificial term, indicating that advection term in sigma coordinates may introduce strong de-mixing.

Although one may hope higher resolution could reduce the artificial source and sink of GPE produced in sigma coordinates, our calculation indicates that it is not the case. As shown in Table 1, increasing the resolution to 0.5° and cutting down the lateral diffusivity in half (500 m^2/s) do not really reduce the GPE source and sink associated with lateral diffusion. On the other hand, increasing the resolution actually enhances the source and sink associated with lateral advection. As shown in Table 1, these terms are nearly doubled for the case of 0.5° resolution. The increase of GPE source and sink associated with lateral advection for the case of higher resolution can be explained as follows. For the case of higher resolution, the horizontal velocity along the sigma surface is larger than that in the lower resolution. As a result, the corresponding change in GPE is enhanced.

The vertical profiles of GPE source and sink are shown in Fig. 1. The results shown in this figure are produced by projecting the GPE source and sink onto the regular z-grid. Thus, the vertical axis is the nominal depth in the original z-grid, and the horizontal axis is the strength of GPE source and sink in each z-coordinate layer. Over all, the source and sink terms are quite large and they reach the maximum at the middle depth (between 1.5–2.5 km) of the ocean.

The strong source and sink in the sigma coordinates is closely linked to the fact that GPE source and sink is strong in deep sigma layers, as shown in Fig. 2. As will be shown through an analytical example in the Appendix, lateral diffusion in sigma coordinate implies mixing of warm water from the top and bottom of seamount/ridge. Due to mixing of water parcels with such large temperature difference, GPE change is quite large.

The meridional distribution of GPE source and sink due to sigma surface stirring and cabbeling is shown in Fig. 3. As discussed in Part III (Huang, 2014c), the distribution of GPE source and sink in both z-coordinates and isopycnal coordinates shows a clear linkage to the strong front associated with strong currents in ACC, Gulf Stream and Kuroshio. However, in sigma coordinates the GPE source and sink has no clear link with these strong fronts.

The strong source and sink of GPE diagnosed from sigma coordinates can be explained in terms of topography and bottom temperature distribution. To demonstrate this idea, we calculate the following two functions of bottom topography and bottom temperature:

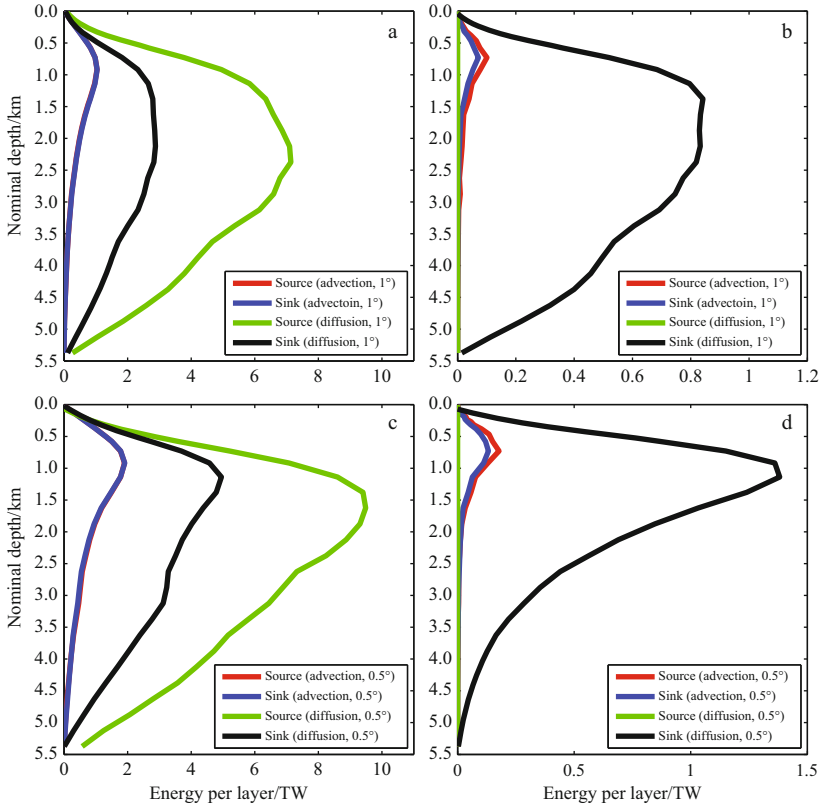

Fig.1. Vertical profiles of GPE source and sink due to stirring associated with lateral diffusion and advection (a) and cabbeling (b) in sigma coordinates, with 1° resolution; the corresponding profiles for the case with 0.5° resolution (c and d). Note that in the left panels the profile of source (marked by red curve) associated with advection is virtually the same as that associated with sink (marked by green curve).

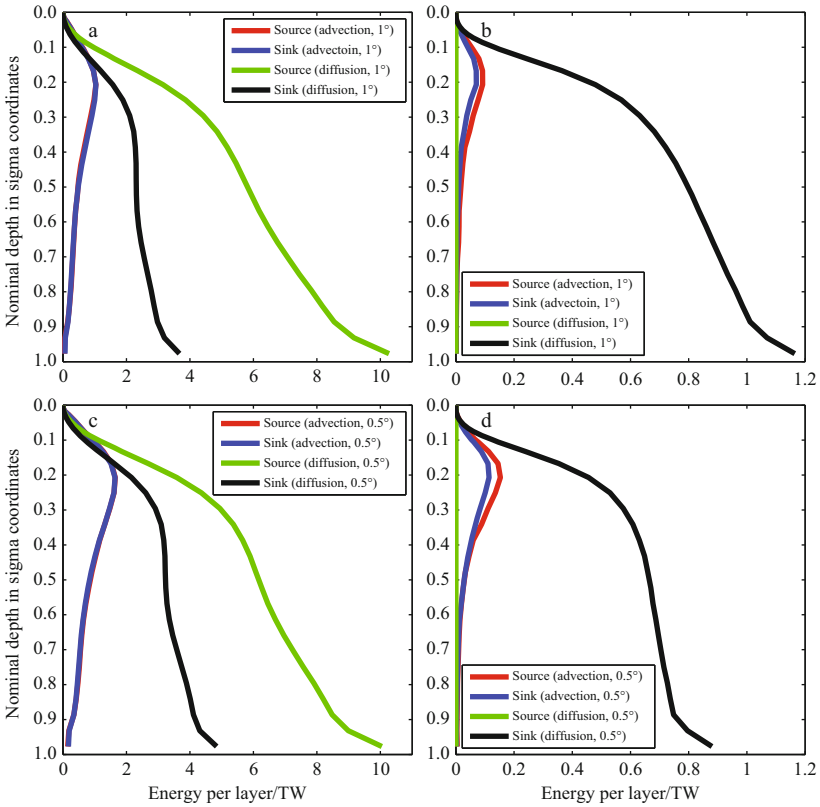

Fig.2. Vertical profiles of GPE source and sink due to stirring (a and c) and cabbeling (b and d) associated with lateral diffusion and advection in sigma coordinates (a and b for 1° resolution, c and d for 0.5° resolution).

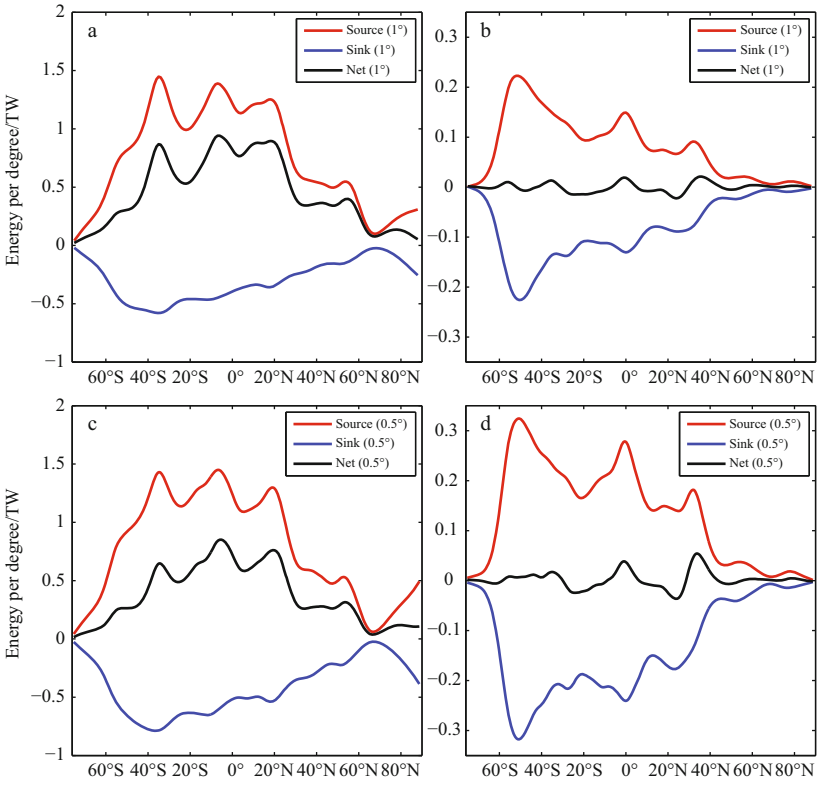

Fig.3. Meridional profiles of GPE source and sink due to stirring associated with lateral diffusion (a) and advection (b) in sigma coordinates, with 1° resolution; the corresponding profiles for the case with 0.5° resolution (c and d).

$$\Delta b(i,j)=\left|z_b(i+1,j)-z_b(i,j)\right|+\left|z_b(i-1,j)-z_b(i,j)\right|+\left|z_b(i,j+1)-z_b(i,j)\right|+\left|z_b(i,j-1)-z_b(i,j)\right|, \quad (27)$$

$$\Delta T(i,j)=\left|T_b(i+1,j)-T_b(i,j)\right|+\left|T_b(i-1,j)-T_b(i,j)\right|+\left|T_b(i,j+1)-T_b(i,j)\right|+\left|T_b(i,j-1)-T_b(i,j)\right|, \quad (28)$$

where z_b and T_b are bottom depth (in km) and bottom temperature (in °C). Note that for grid points on land, the corresponding depth and temperature are set to zero, so that they do not contribute.

The meridional or zonal integration of these two functions are defined as

$$\sum\nolimits_{\text{latitude}}\Delta z=\sum_{j=1}^{165}{}_{i=\text{const.}}\Delta z(i,j)\ ,\ \sum\nolimits_{\text{latitude}}\Delta T=\sum_{j=1}^{165}{}_{i=\text{const.}}\Delta T(i,j)\ , \quad (29)$$

$$\sum\nolimits_{\text{longitude}}\Delta z=\sum_{i=1}^{360}{}_{j=\text{const.}}\Delta z(i,j)\ ,\ \sum\nolimits_{\text{longitude}}\Delta T=\sum_{i=1}^{360}{}_{j=\text{const.}}\Delta T(i,j)\ . \quad (30)$$

The results are shown in Fig. 4. A high value shown in this figure indicates that the bottom temperature difference along a fixed latitudinal and longitudinal band is high.

For example, $\sum_{\text{latitude}}\Delta T$ shown in Fig. 4a is high at low latitudes and very low at high latitudes. This is due to the fact that deep and bottom water is formed at high latitudes where cold temperature at late winter produces cold and dense water. Cold water formed at high latitudes spreads towards low latitudes. Thus, bottom temperature at high latitude is quite uniform. On the other hand, cold water is carried out to low latitudes, mostly in forms of deep boundary currents. Cold bottom water spreads towards the interior ocean through long and slow processes. Hence, bottom water in the ocean interior away from the side boundary can be much warmer than that near the boundary current. As a result, the zonally accumulated bottom temperature difference at low latitudes is quite large. Consequently, the GPE source and sink due to stirring and cabbeling associated with sigma diffusion and advection is large at low latitudes.

The zonal distribution of GPE source and sink due to stirring and cabbeling associated with sigma diffusion and advection is shown in Fig. 5. Here again, there are two bands of high value, one near 120°–140°E and one near 60°–90°W. Comparing these panels with the right panels in Fig. 4 reveals that these high value bands are closely related to the high $\sum_{\text{latitude}}\Delta T$ and $\sum_{\text{latitude}}\Delta z$ bands in the western Pacific Ocean and western Atlantic Ocean. The high value of $\sum_{\text{latitude}}\Delta T$ is probably linked to the existence of deep western boundary currents carrying cold bottom water and the relatively warm water in the ocean interior. In the eastern part of the basin, bottom temperature contrast is much smaller in comparison.

The GPE source and sink due to cabbeling associated with sigma diffusion and cabbeling is shown in Figs 6 and 7. Once again, the high value bands are not linked to any density fronts in the ocean. Instead, they seem to be linked to the same bands of high accumulated bottom temperature difference and bottom depth difference. In the meridional figure (Fig. 6) they ap-

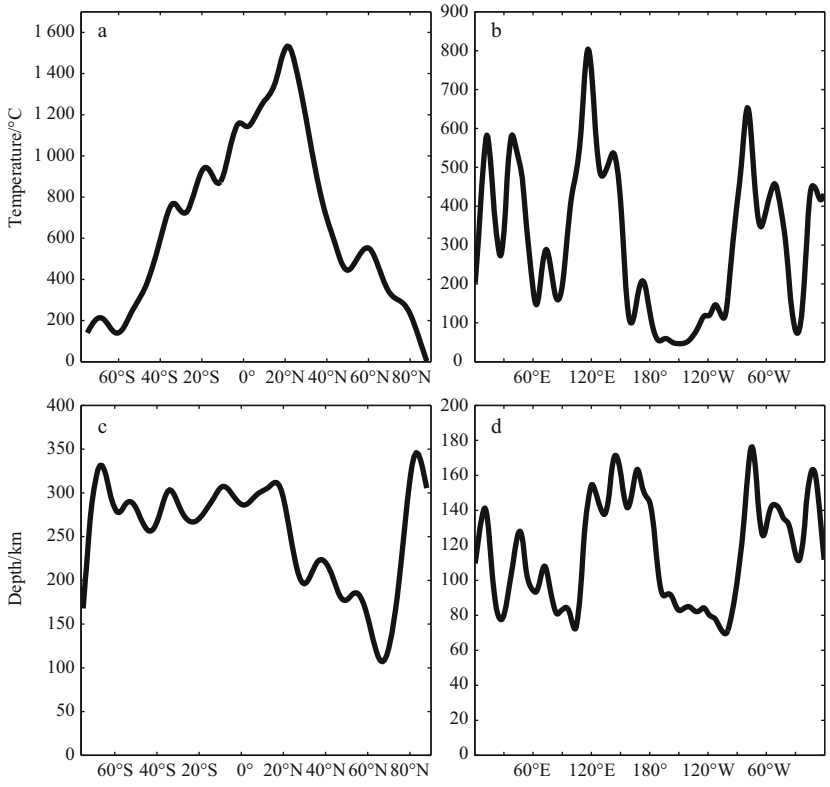

Fig.4. Meridionally and zonally accumulated difference in bottom temperature and depth. a. Meridionally accumulated bottom temperature difference, b. zonally accumulated bottom temperature difference, c. meridionally accumulated bottom depth difference and d. zonally accumulated bottom depth difference.

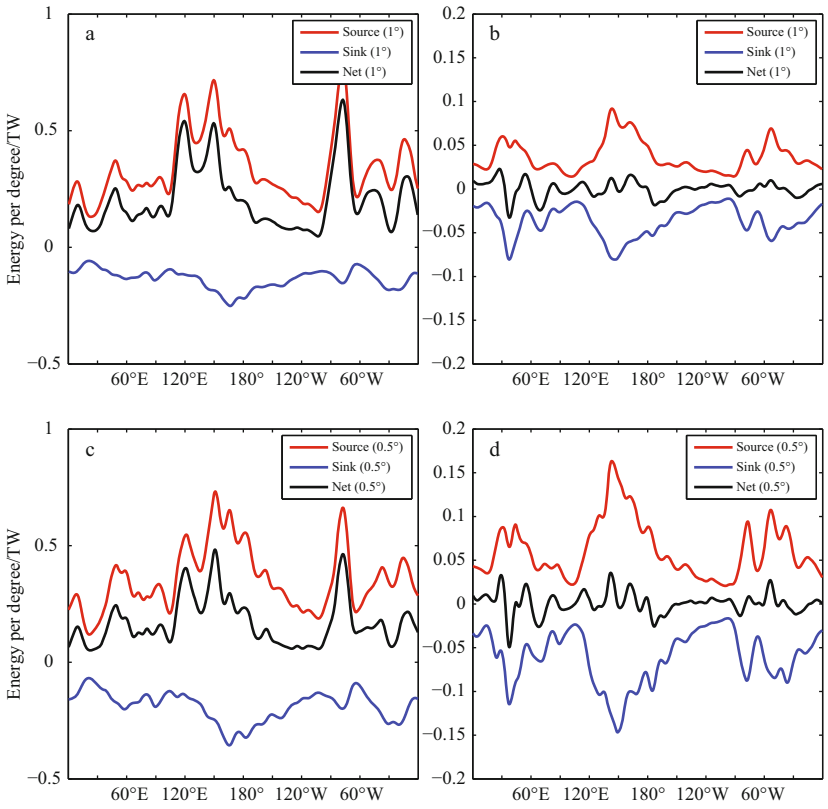

Fig.5. Zonal profiles of GPE source and sink due to stirring associated with lateral diffusion (a) and advection (b) in sigma coordinates, with 1° resolution; the corresponding profiles for the case with 0.5° resolution (c and d).

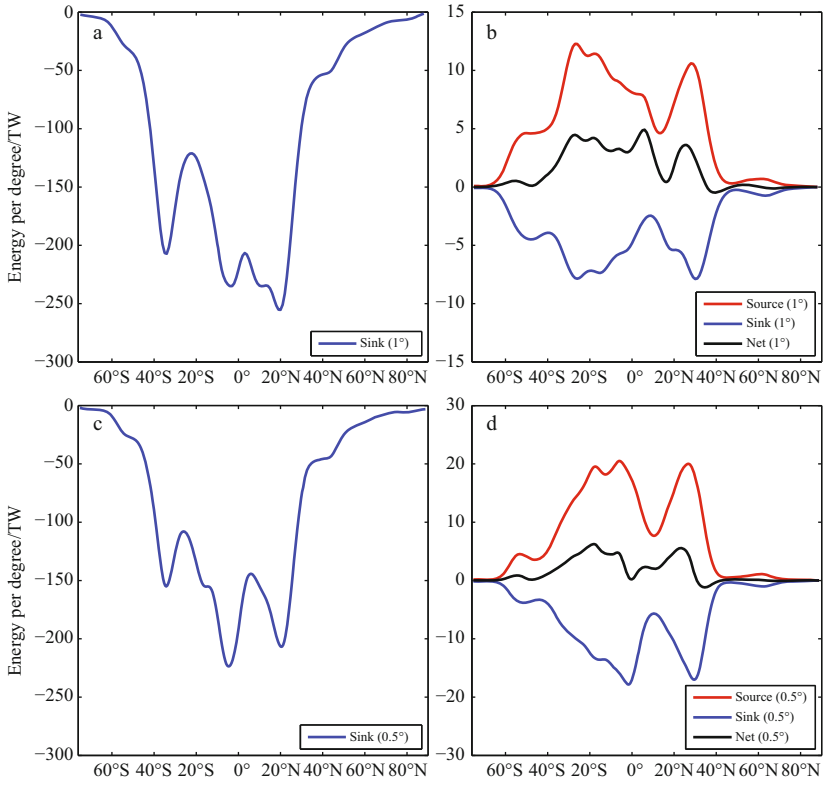

Fig.6. Meridional profiles of GPE source and sink due to cabbeling associated with lateral diffusion (a) and advection (b) in sigma coordinates, with 1° resolution; the corresponding profiles for the case with 0.5° resolution (c and d).

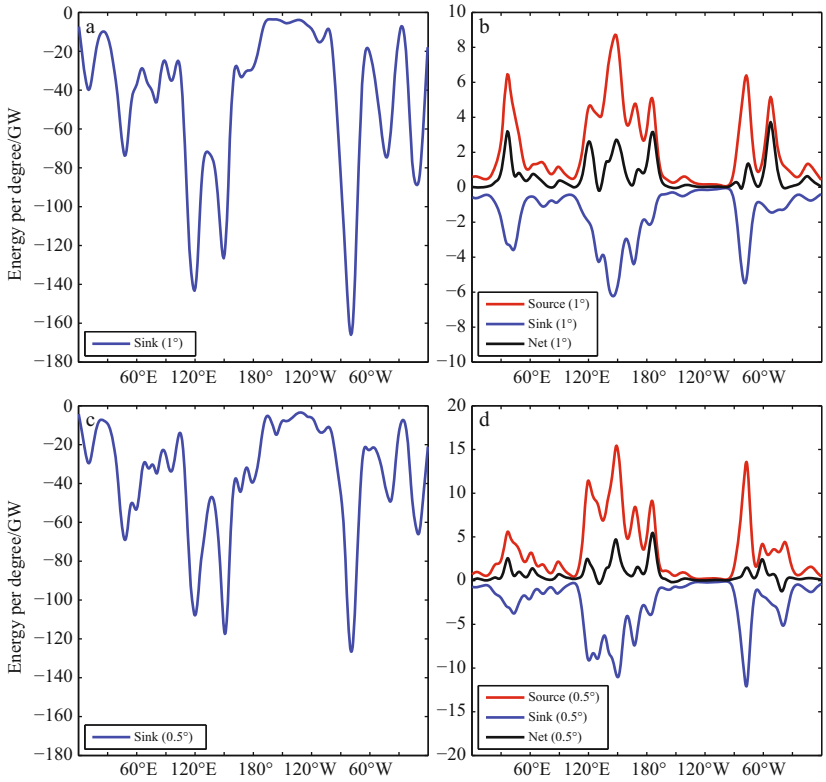

Fig.7. Zonal profiles of GPE source and sink due to cabbeling associated with lateral diffusion (a) and advection (b) in sigma coordinates, with 1° resolution; the corresponding profiles for the case with 0.5° resolution (c and d).

pear along 120–140°E and near 60–90°W; in the zonal figure, they appear in the western part of the Pacific Ocean and Atlantic Ocean. There is very strong source of GPE due to cabbeling associated with sigma advection. Such source indicates the large numerical demixing in the sigma coordinates.

Zonal profiles of GPE source and sink due to cabbeling associated with lateral diffusion and advection are shown in Fig. 7. There seems no clear connection with water property distribution as discussed in the case of isopycnal diffusion and advection in Part III (Huang, 2014c).

2.3 *An idealized show case*

In order to demonstrate the idea that diffusion and advection along the traditional sigma surfaces may induce large artificial errors we carried out the following calculations.

Using the SODA data, the horizontal mean temperature and salinity profiles are calculated, as shown in Fig. 8. From such vertical profiles of temperature and salinity we can generate three dimensional temperature and salinity fields for three different coordinates, z-coordinates, isopycnal coordinates and sigma coordinates, such datasets will be labeled as SODA-HM

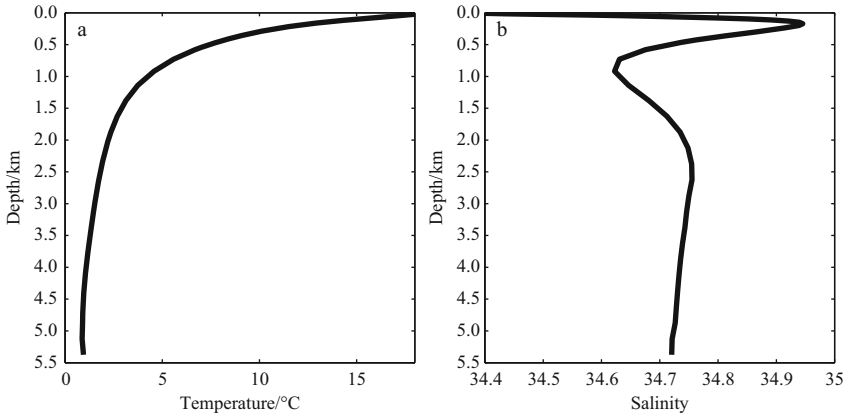

Fig.8. Vertical profiles of horizontal mean temperature (a) and salinity (b) obtained from SODA data.

(horizontal mean).

Since both temperature and salinity are homogeneous in all horizontal surfaces, isopycnal surfaces in this dataset are all horizontal, i.e., z-coordinates and isopycnal coordinates are the same for this dataset. As an example, the temperature and salinity distribution along 29.5°W in the SODA data and SODA-HM data are shown in Figs 9 and 10. The upper panels of these figures show temperature and salinity distribution in the SODA data; while the lower panels of these figures show temperature and salinity distribution in the SODA-HM data.

From Figs 9c and 10c, it is clear that there is nothing to be mixed horizontally. Since there is no horizontal gradient of temperature and salinity, isopycnal surfaces are also horizontal. As a result, horizontal or isopycnal diffusion and advection lead to no change in the system. Therefore, GPE source and sink due to lateral diffusion and advection in the z-coordinates and isopycnal coordinates are exactly zero.

On the other hand, there is large gradient of temperature and salinity on the sigma surfaces, as shown in Figs 9d and 10d. Lateral diffusion of such fields should certainly lead to great change of GPE. In addition, lateral advection of such fields can also generate great source and sink of GPE.

Applying the formulae derived above to the SODA and SODA-HM data, the GPE source and sink due to stirring and cabbeling associated with sigma diffusion and advection can be calculated, and the results are shown in Table 2.

These results indicate that there is a huge amount of GPE source and sink due to stirring and cabbeling associated with sigma diffusion and advection. For each item listed in Table 2, the GPE source and sink in sigma coordinates does not seem to change much, whether we use the original SODA data, which represents the real situation in the world oceans, or if we use the SODA-HM data, which has no horizontal temperature and salinity gradient in z-coordinates.

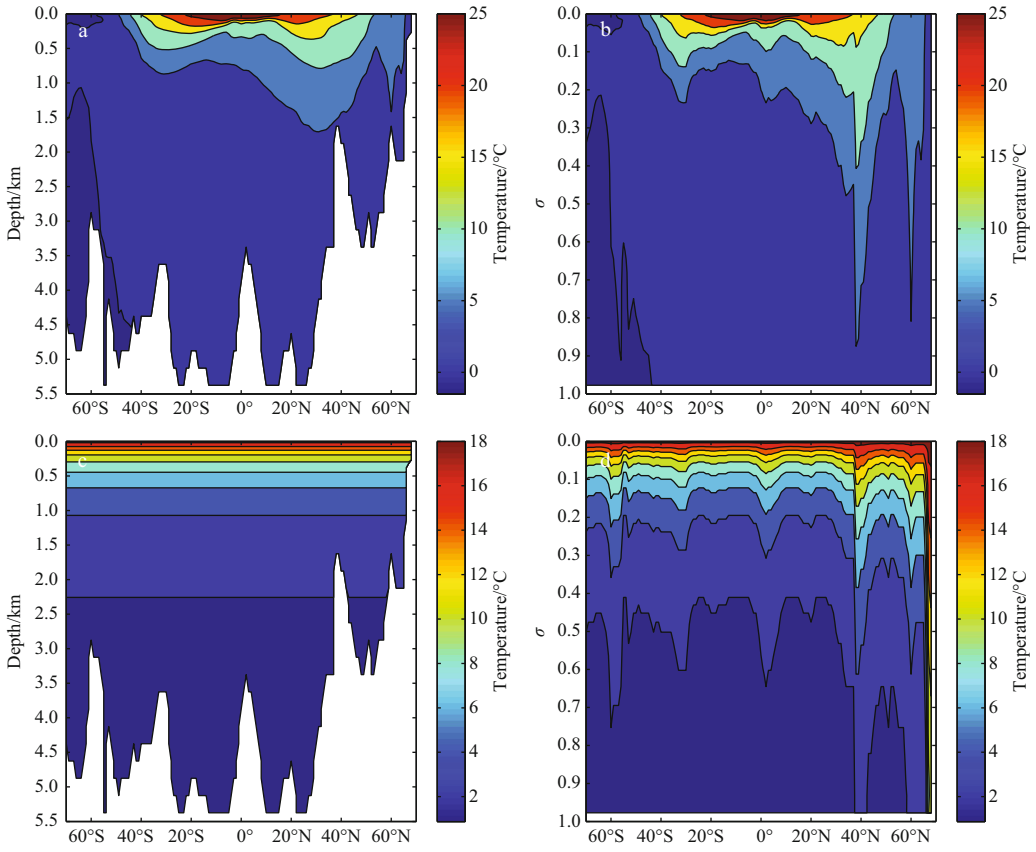

Fig.9. Temperature distribution along 29.5°W, a and c are in z-coordinates, b and d are in sigma coordinates; a and b are from the SODA data, c and d are from the SODA-HM data.

Table 2. GPE source and sink in sigma coordinates (TW), based SODA and SODA-HM with 1° resolution

Terms	Data	Stirring			Cabbeling		
		Source	Sink	Net	Source	Sink	Net
Diffusion	SODA	123.8	−48.9	74.9	0	−16.0	−16.0
	SODA-HM	130.2	−52.3	77.9	0	−15.2	−15.2
Advection	SODA	13.4	−13.3	0.16	0.78	−0.55	0.23
	SODA-HM	11.8	−11.6	−0.20	0.43	−0.35	0.18

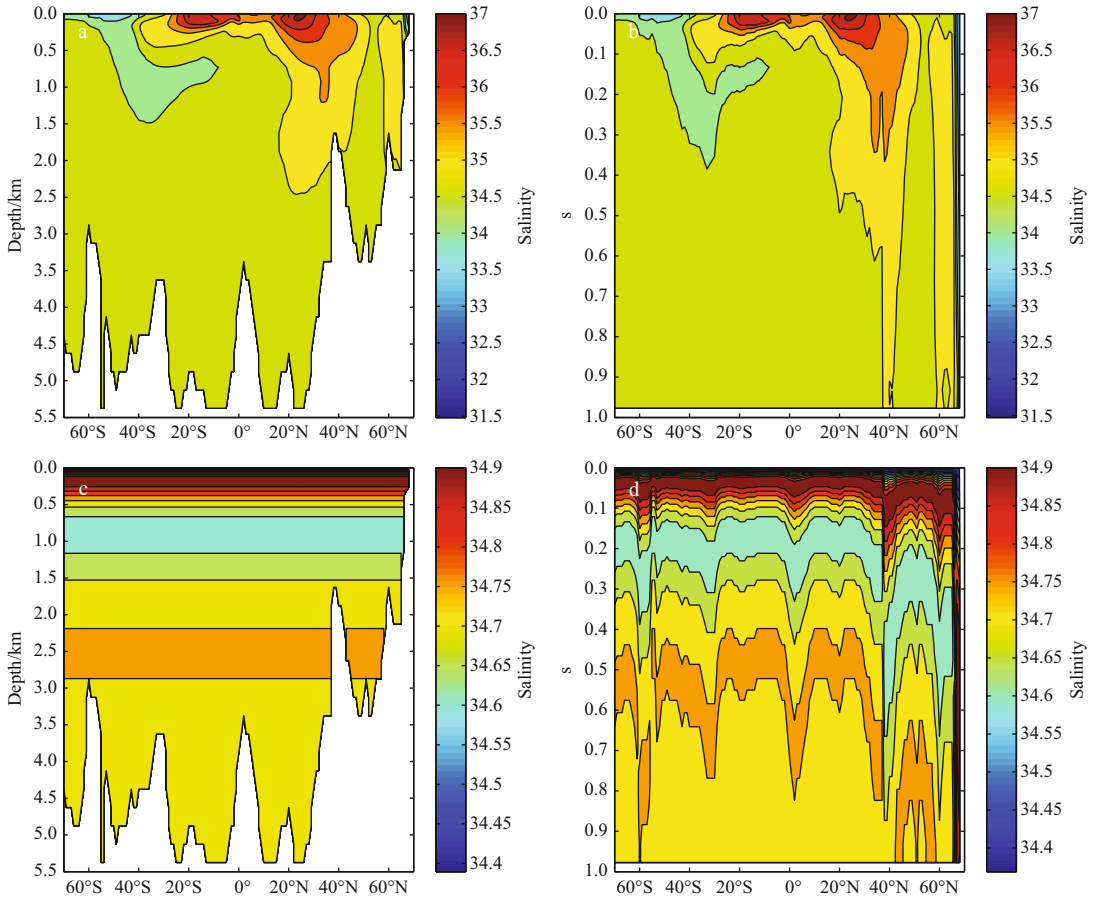

Fig.10. Salinity distribution along 29.5°W, a and c are in *z*-coordinates, b and d are in sigma coordinates; a and b are from the SODA data, c and d are from the SODA-HM data.

Comparing the meridional distribution of GPE source and sink due to stirring associated with sigma diffusion (Figs 11a and c) shows that the pattern of source and sink obtained from these two datasets are quite similar, with the only difference that the strength of GPE source and sink in SODA-HM is reduced. Since there is no horizontal temperature and salinity gradient in the SODA-HM data, GPE source and sink shown in Fig. 11c is completely artificial. The fact that profiles in Figs 11a and c are similar implies that most part of the GPE source and sink presented in Fig. 11a may be originated from the same source—the unphysical assumption of diffusion along sigma surfaces.

The meridional distribution of GPE source and sink due to stirring associated with sigma advection (Figs 11b and d) is even more resemble to each other, including both the amplitude and pattern. The similarity between these two results implies that most of such GPE source and sink is artificial.

The zonal distribution of GPE source and sink due to stirring associated with sigma diffusion and advection is shown in Fig. 12. They resemble each other, including both the amplitude and pattern. The similarity between these two results implies that most of the GPE source and sink in the sigma coordinates model is artificial.

The meridional and zonal distribution of GPE source and sink due to cabbeling associated with sigma diffusion and advection is shown in Figs 13 and 14. The sink of GPE due to cabbeling associated with diffusion for the case of SODA-HM is all artificial. The large amplitude of such sink term indicates that GPE sink due to cabbeling associated with diffusion in sigma coordinates is artificial.

2.4 *Summary*

The GPE source and sink due to stirring and cabbeling associated with sigma diffusion and advection is discussed in this section. These terms are too big compared with the upper bound of 0.1 TW postulated above. The zonal and meridional distributions of GPE source and sink seem to be unrelated to the water property distribution. Instead, as shown in Section 2.3, even for the case with no horizontal gradient of temperature and salinity, sigma diffusion and advection can still produce a huge amount of GPE source and sink. This point is also further explored in the Appendix. Therefore, we come to the conclusion that strong GPE source and sink due to sigma diffusion is very artificial and it is directly linked to the assumption of eddy diffusion and advection along sigma surfaces. The calculation of this section raises serious questions whether simulating eddy diffusion and advection along sigma surface is an acceptable way of modeling oceanic processes.

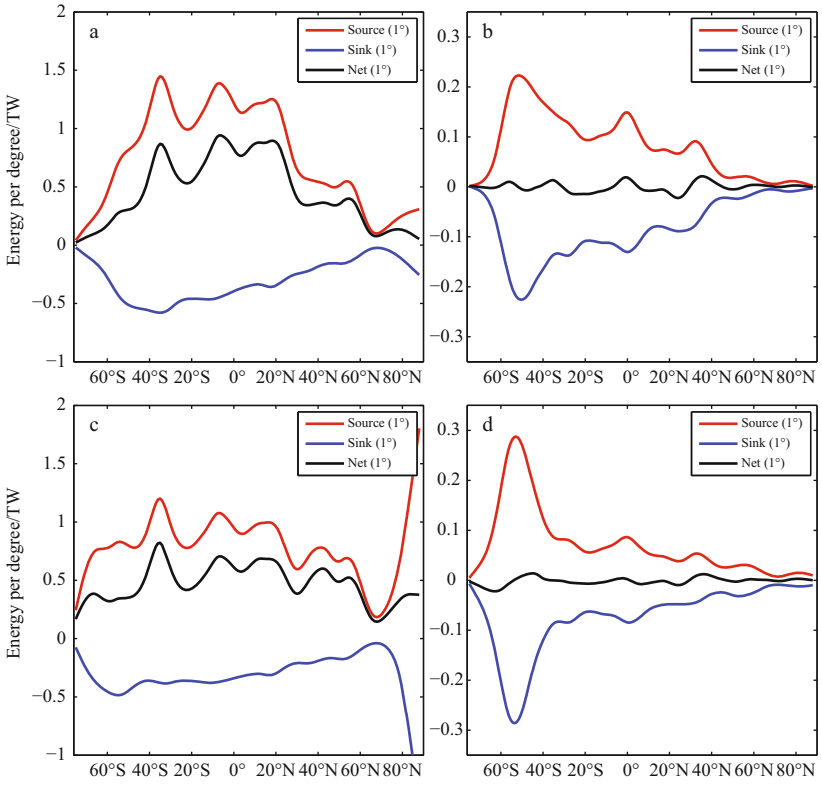

Fig.11. Meridional distribution of GPE source and sink due to stirring associated with sigma diffusion (a and c) and advection (b and d), obtained from SODA (a and b) and SODA-HM (c and d).

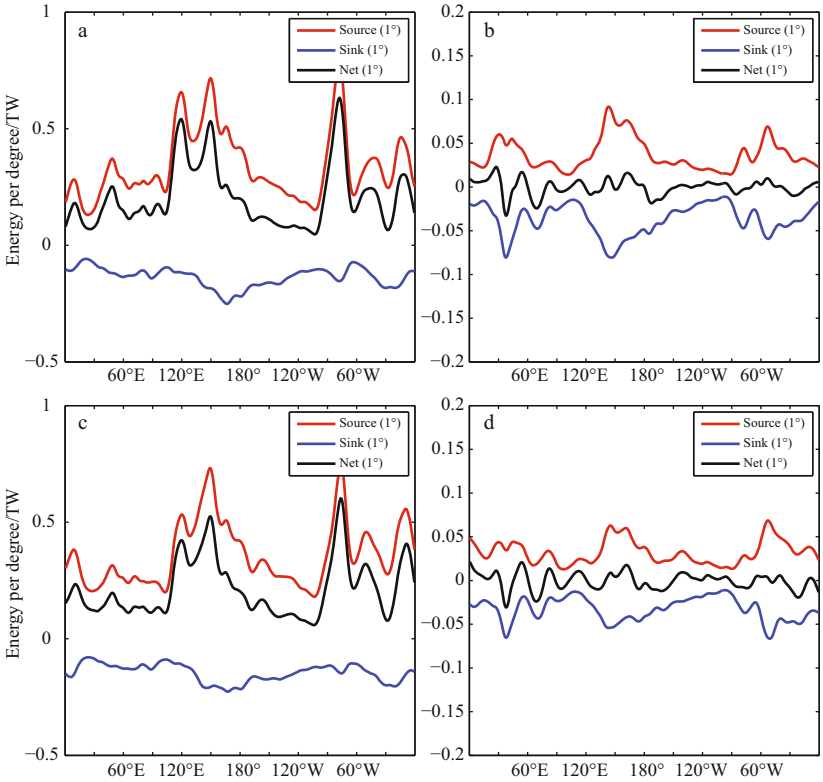

Fig.12. Zonal distribution of GPE source and sink due to stirring associated with sigma diffusion (a and c) and advection (b and d), obtained from SODA (a and b) and SODA-HM data (c and d).

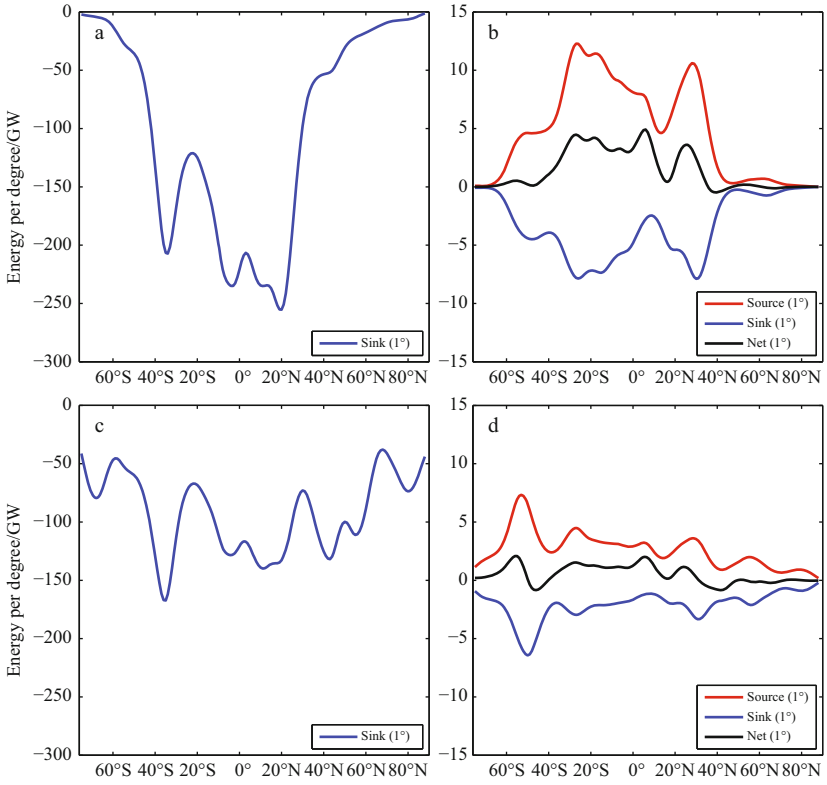

Fig.13. Meridional distribution of GPE source and sink due to cabbeling associated with sigma diffusion (a and c) and advection (b and d), obtained from SODA (a and b) and SODA-HM data (c and d).

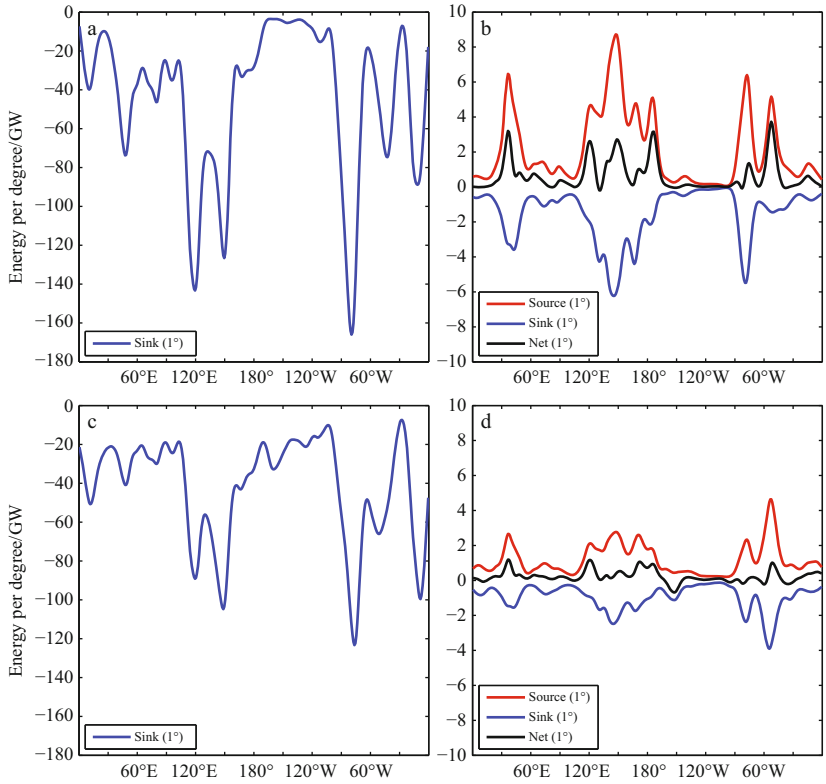

Fig.14. Zonal distribution of GPE source and sink due to cabbeling associated with sigma diffusion (a and c) and advection (b and d), obtained from SODA (a and b) and SODA-HM data (c and d).

3 Comparison of eddy diffusion/advection in different coordinates

The GPE source and sink associated with lateral diffusion and advection has been discussed in the study, and this is a continuation of Huang (2014a, b and c), and the previous parts will be denoted as Part I, Part II, and Part III. In this section, we will explore the difference between results obtained from three coordinates. Among the many differences between these coordinates, there is a major difference in terms of how to deal flow near a steep topography. Due to dynamical constraints for large-scale circulation, the primary flow near the topography is quasi-geostrophic; thus, its direction tends to be quasi-isopycnal (or close to quasi-horizontal). There can be secondary or even tertiary flow near the topography; however, such components should be rather weak in general. As a result, near the topography, model based on geopotential coordinates or isopycnal coordinates have no effective grids inside the topography, i.e., in these coordinates, lateral diffusion or advection is blocked by topography (Fig. 15).

On the other hand, sigma grid is completely free of topography blocking, as shown in Fig. 15. In this case, lateral diffusion and advection going up and down steep topography is permitted in a sigma coordinate model. As such, lateral diffusion and advection in sigma coordinate models allows the exchange of relatively warm water at shallow levels with relatively cold water from deeper levels, as shown in Fig. 15. Even if we turn off the lateral eddy diffusion, there is still the lateral advection in the model. As shown in Part II, if the horizontal velocity is not in line with the local coordinate axis, there will be numerical advection error introduced through advection of tracer from the side grid points, shown by the red and blue arrows in Fig.16. As analyzed in Appendix, such a cross-isobaths exchange can produce large source and sink of GPE. Except for some special situations, such cross-isobaths exchange is dynamically forbidden; thus, simulating flow near topography in such a way may be the unphysical aspect of sigma coordinate models.

The rest of this paper is organized as follows. The difference in GPE source and sink diagnosed from these three coordinates is analyzed in Section 3.1. In general, GPE source and sink can change greatly with smoothing applied to data, and this is explored in Section 3.2. Finally, we draw conclusion in Section 4.

3.1 *GPE source/sink in these three coordinates*

In order to see the difference between these three coordinates, we made the following composite Table 3. For many items, the ratio between the isopycnal coordinates, the z-coordinates and the sigma coordinates is 1:100:1 000.

The comparison of individual profiles is shown in the fol-

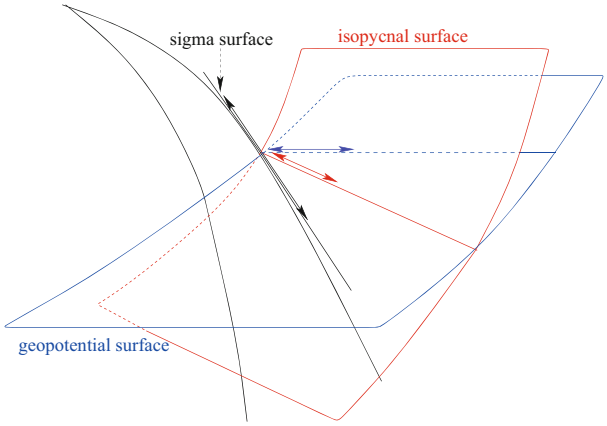

Fig.15. Three coordinates plot against a seamount.

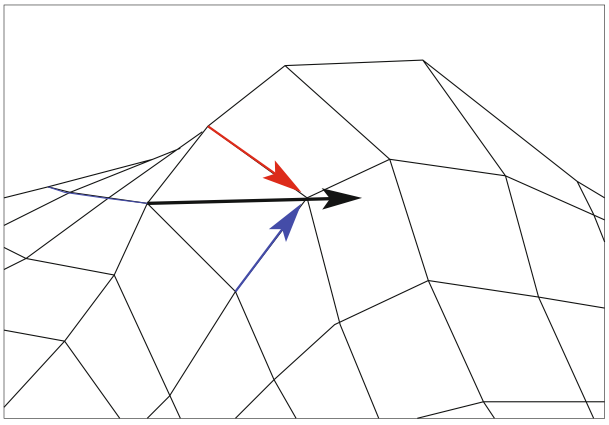

Fig.16. Flow adjacent to a seamount on a sigma coordinates.

Table 3. GPE source and sink (GW) due to lateral stirring & advection

Coor.	Terms	Grids/(°)	Stirring			Cabbeling		
			Source	Sink	Net	Source	Sink	Net
Isopy.	Diffusion	1.0	37	−76	−39	0	−89	−89
		0.5	23	−44	−21	0	−55	−55
	Advection	1.0	339	−337	2	28	−22	6
		0.5	374	−390	−16	17	−15	2
z	Diffusion	1.0	8 422	−8 410	12	0	−366	−366
		0.5	6 452	−6 456	−4	0	−233	−233
	Advection	1.0	4 484	−4 040	444	120	−106	14
		0.5	4 137	−4 619	−482	75	−67	8
Sigma	Diffusion	1.0	123 780	−48 891	74 889	0	−16 042	−16 042
		0.5	129 190	−67 560	61 630	0	−13 100	−13 100
	Advection	1.0	13 290	−13 348	−158	779	−547	232
		0.5	22 168	−21 864	304	1 229	−975	254

Notes: K=1 000 m^2/s for 1° resolution, and K=500 m^2/s for 0.5° resolution; analysis is based on 50-year mean SODA data salinity, temperature and horizontal velocity.

lowing figures. Note that in order to put results obtained from these three different coordinates on the same plot, we have to multiply the results from z-coordinates and sigma coordinates with a factor between 0.001 and 0.1. The vertical profiles of GPE source/sink due to stirring associated with lateral diffusion are shown in Fig. 17. Overall, vertical profiles in isopycnal coordinates is more surface intensified; on the other hand, vertical profiles in z-coordinates and sigma coordinates often reach their maximum at the middle depth.

The vertical profiles of GPE source/sink due to cabbeling associated with lateral diffusion are quite interesting. As shown in Fig. 18a, for the case with 1° resolution, profiles in both the isopycnal and z coordinates reach the maximum above 1km; while in the sigma coordinates, the profile reaches the maximum at the middle depth (1.5–2.5 km). For the case with 0.5° resolution, the corresponding maxima are compressed towards the surface. Once again, the vertical profile in the sigma coordinates penetrates deeper.

Vertical profiles of GPE source and sink due to stirring associated with lateral advection are shown in Fig. 19. Although the magnitude of this term in these three coordinates is quite different, the corresponding profiles are rather similar. Note that the source profile and the sink profile seem to be the same, except the sign. This may lead people to an incorrect conclusion that in terms of GPE source and sink numerical errors induced by the advection nearly cancel each other, and leave very little dynamical consequence. However, this may not be the case, as will be shown shortly.

Vertical profiles of GPE source and sink due to cabbeling associated with lateral advection are shown in Fig. 20. The magnitude of this term in these three coordinates is quite different. In addition, the profiles in sigma coordinates penetrates much deeper than in other two coordinates. The most important point to be seen from this figure is as follows. In all three coordinates, cabbeling associated with lateral advection leads to large amount of GPE source. Physically, such positive source of GPE due to cabbeling indicates that lateral advection actually leads to de-mixing; as a result of such de-mixing, the density of the water produced after subscale diffusion associated with advection is lighter than the original water parcels. Thus, such positive source of GPE due to cabbeling associated with lateral advection is unphysical, and we should try to eliminate such problem in numerical simulation. Furthermore, the magnitude of the GPE source and sink due to stirring and cabbeling associated with lateral advection may be used as a criterion to evaluate the model performance in terms of simulating lateral advection in the ocean.

Meridional profiles of GPE source and sink due to stirring

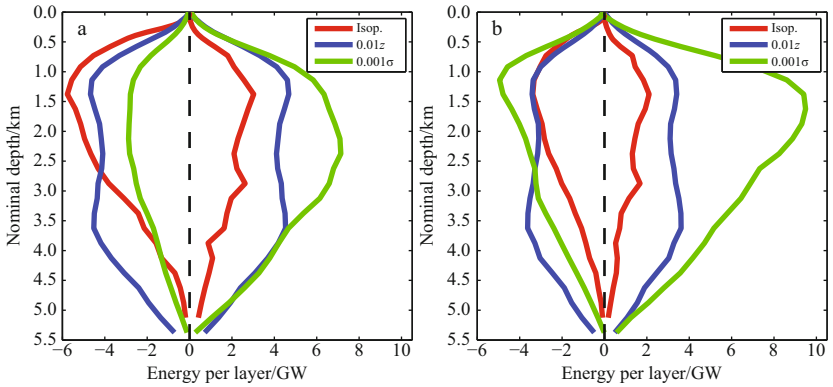

Fig.17. Vertical profiles of GPE source and sink due to stirring associated with lateral diffusion in three different coordinates, with 1° (a) and 0.5° (b) resolution.

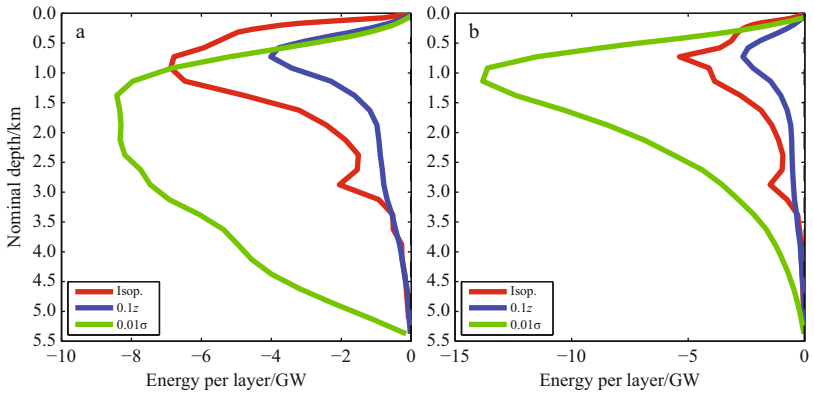

Fig.18. Vertical profiles of GPE source and sink due to cabbeling associated with lateral diffusion in three different coordinates, with 1° (a) and 0.5° (b) resolution.

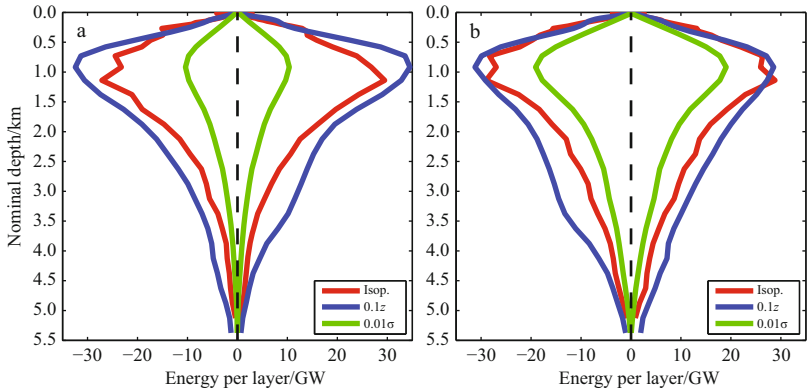

Fig.19. Vertical profiles of GPE source and sink due to stirring associated with lateral advection in three different coordinates, with 1° (a) and 0.5° (b) resolution.

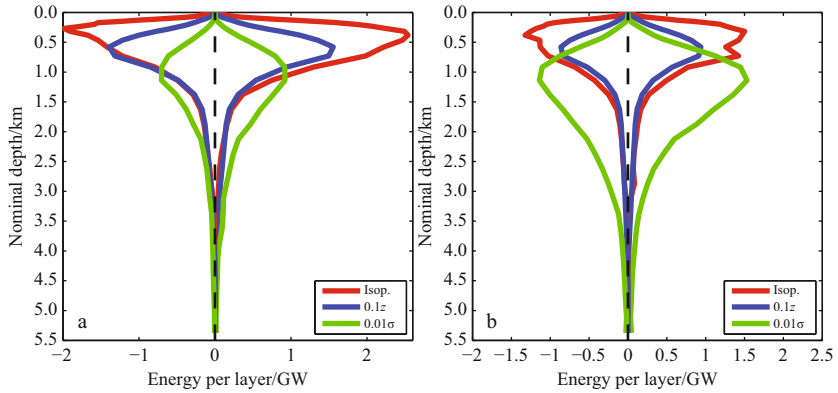

Fig.20. Vertical profiles of GPE source and sink due to cabbeling associated with lateral advection in three different coordinates, with 1° (a) and 0.5° (b) resolution.

associated with lateral diffusion are shown in Fig. 21. The magnitude of this term in these three coordinates is 1 000 times in difference. Around the latitude of ACC, there is strong sink of GPE and weak source due to stirring associated with lateral diffusion in isopycnal coordinates, which reflects the strong front associated with the strong currents. However, in the z-coordinates, the strength of source and sink is about the same. In the sigma coordinates, the corresponding source is much larger than the sink. In addition, the peaks of source and sink appear at low and middle latitudes. As argued in Section 1, this is due to the artificial nature of lateral diffusion in sigma coordinates. Instead of diffusion linked to the strong properties fronts, lat-

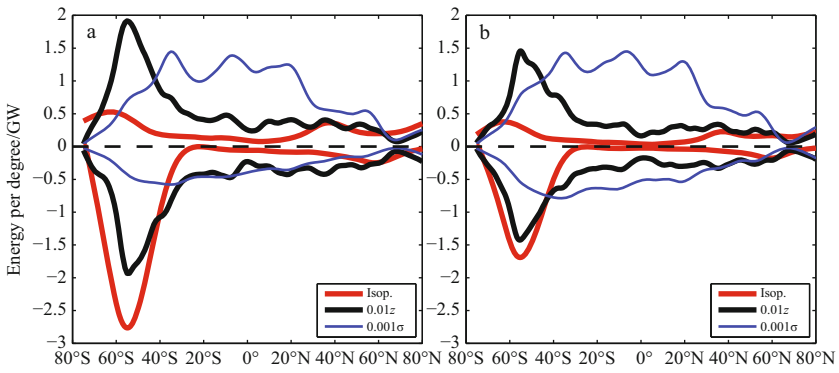

Fig.21. Meridional profiles of GPE source and sink due to stirring associated with lateral diffusion in three different coordinates, with 1° (a) and 0.5° (b) resolution.

eral diffusion in sigma coordinates is mostly linked to the strong bottom temperature difference along the sigma surfaces. When the horizontal grid size is reduced to 0.5° and the corresponding lateral diffusivity cut to 500 m^2/s, the source and sink in isopycnal coordinates is reduced; however, the corresponding terms in sigma coordinates are slightly increased. Thus, at least for the present two cases, increasing the horizontal resolution does not help to reduce the artificial diffusion in the sigma coordinates.

Meridional profiles of GPE sink due to cabbeling associated with lateral diffusion are shown in Fig. 22. The GPE sink in isopycnal coordinates is near the level of acceptable; on the other hand, the GPE sink in both z and sigma coordinates are too large and not acceptable. In particular, the meridional distribution of GPE sink in sigma coordinates is completely out of the right place, as shown in Fig. 22. As analyzed in Section 1, such a meridional distribution is linked to the strong bottom temperature gradient at low and middle latitudes.

Meridional profiles of GPE source and sink due to stirring associated with lateral advection are shown in Fig. 23. Although the GPE source and sink profiles look similar, the profile in sigma coordinates has a noticeable secondary peak near the equator. This secondary peak does not exist in the isopycnal coordinates; thus, it seems an artificial part of the simulation.

Meridional profiles of GPE source and sink due to cabbeling associated with lateral advection are shown in Fig. 24. Here again, results from the sigma coordinates have large peaks of source and sink of GPE at lower latitudes. These peaks are not directly linked to physical property distribution, and they are apparently artifacts of the sigma models.

Meridional profiles of GPE source and sink due to stirring associated with lateral diffusion are shown in Fig. 25. The magnitude of this term in these three coordinates is very different. In isopycnal coordinates, peaks of GPE source and sink appear at the Atlantic sector, and they seem to be linked to the strong physical property gradients there. In z-coordinates simulation, GPE source and sink have strong peaks in the Pacific sector, where the corresponding source and sink in isopycnal coordinates is quite low. In sigma coordinates, the major peaks of source appear in the western Pacific and the Atlantic Oceans. In comparing with the source and sink distribution obtained from isopycnal coordinates, these peaks seem artificial.

Zonal profiles of GPE sink due to cabbeling associated with lateral diffusion are shown in Fig. 26. The distribution in isopycnal coordinates reflects the fact that there is strong thermohaline circulation in the Atlantic Ocean. The profile of sink in z-coordinates shares similar feature as in the isopycnal coordinates, although the corresponding magnitude is about ten times larger. On the other hand, the GPE sink in the sigma coordinates is about 200 times larger. Furthermore, the strong peaks in the western Pacific and western Atlantic Oceans seem unrelated to the local thermohaline circulation.

Zonal profiles of GPE source and sink due to stirring associ-

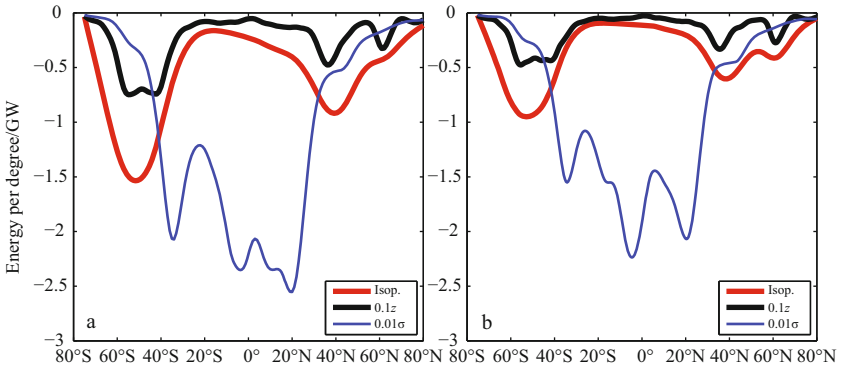

Fig.22. Meridional profiles of GPE source and sink due to cabbeling associated with lateral diffusion in three different coordinates, with 1° (a) and 0.5° (b) resolution.

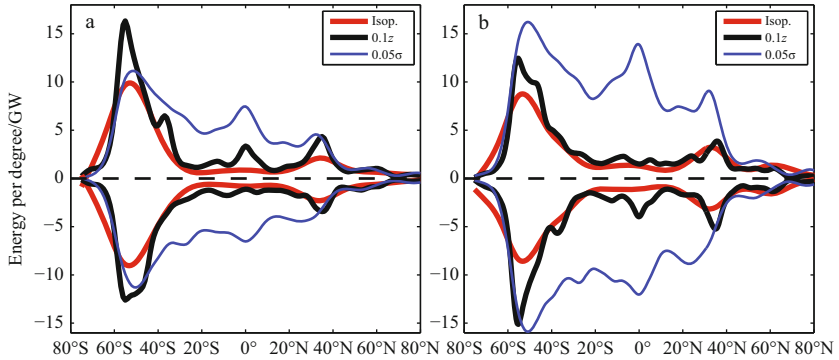

Fig.23. Meridional profiles of GPE source and sink due to stirring associated with lateral advection in three different coordinates, with 1° (a) and 0.5° (b) resolution.

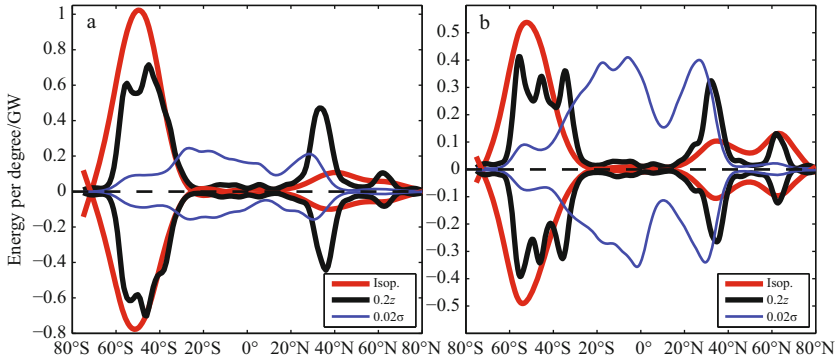

Fig.24. Meridional profiles of GPE source and sink due to cabbeling associated with lateral advection in three different coordinates, with 1° (a) and 0.5° (b) resolution.

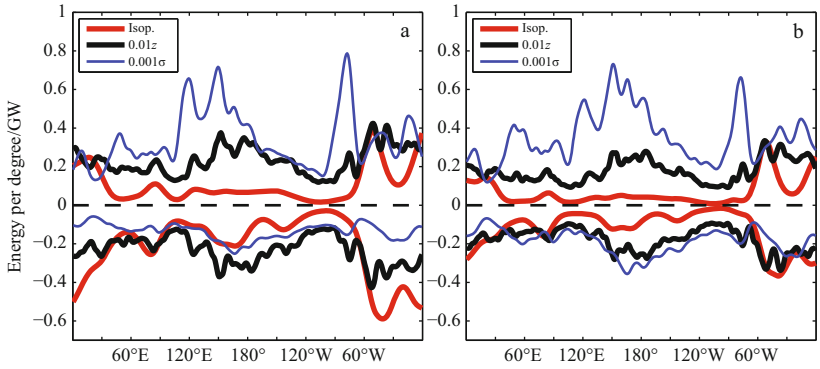

Fig.25. Zonal profiles of GPE source and sink due to stirring associated with lateral diffusion in three different coordinates, with 1° (a) and 0.5° (b) resolution.

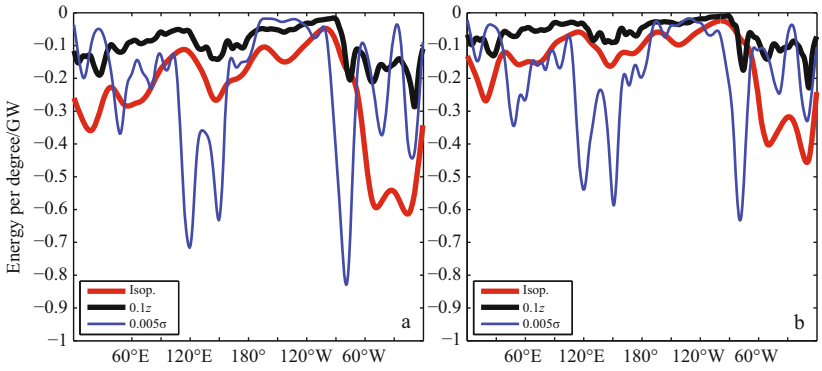

Fig.26. Zonal profiles of GPE source and sink due to cabbeling associated with lateral diffusion in three different coordinates, with 1° (a) and 0.5° (b) resolution.

ated with lateral diffusion are shown in Fig. 27. Overall, source and sink of GPE in the z-coordinates and sigma coordinates is 10 times and 100 times larger than that from isopycnal coordinates. The similarity of patterns reflects the fact that the source and sink due to advection is linearly proportional to horizontal velocity, which has similar patterns in these three coordinates.

Zonal profiles of GPE source and sink due to cabbeling associated with lateral advection are shown in Fig. 28. Here again, the magnitude of source and sink in these three coordinates is quite different. The similarity of patterns reflects the fact that the source and sink due to advection is linearly proportional to horizontal velocity, which has similar patterns in these three coordinates.

3.2 *The effect of data smoothing*

Note that the results shown above were obtained with the

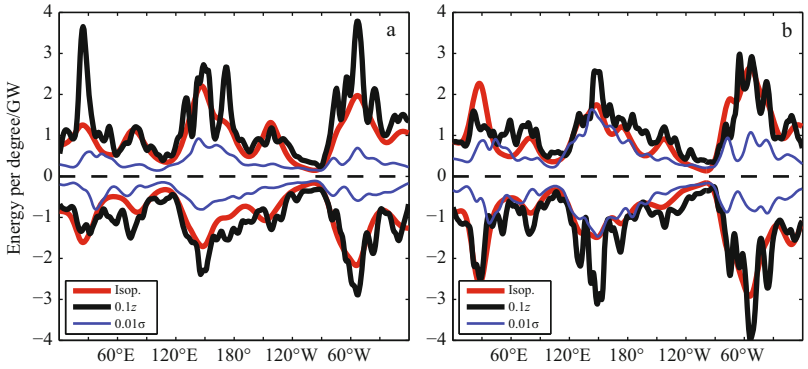

Fig.27. Zonal profiles of GPE source and sink due to stirring associated with lateral advection in three different coordinates, with 1° (a) and 0.5° (b) resolution.

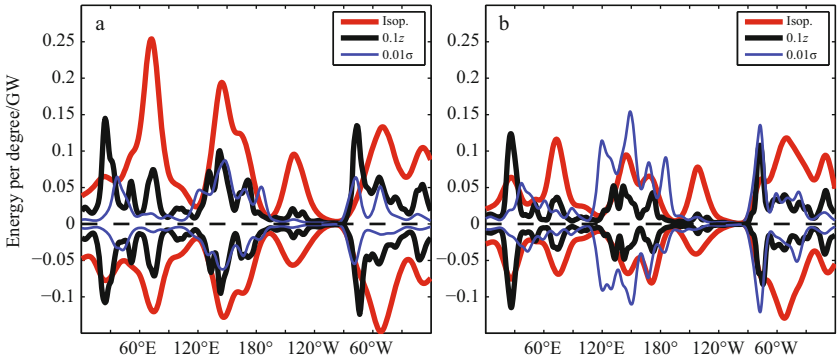

Fig.28. Zonal profiles of GPE source and sink due to cabbeling associated with lateral advection in three different coordinates, with 1° (a) and 0.5° (b) resolution.

least amount of smoothing on the original 50-year mean SODA data. With smoothing on data, one can certainly reduce the corresponding GPE source and sink. For example, we applied the standard Matlab smoothing function "*fsmooth*" to each layer of data, the results change gradually, depending on how many times the smoothing function was applied, see Table 4.

Of course, one should not smooth the data, unless it is necessary. However, the point of carrying out this set of experiment is to demonstrate that data with less smoothing should gives rise to higher GPE source and sink. Since our calculation is based on the 50-year mean SODA climatology data, it is highly smoothed. It is thus speculated that if the same formulae apply to the annual mean, or even instantaneous data obtained from numerical simulation, the corresponding GPE source and sink would be greatly increased.

4 Summary and conclusions

In this study we went through a great length in exploring fundamental dynamic issues related to quasi-horizontal diffusion and advection in the ocean and the corresponding parameterization in numerical models. The major points in our study are summarized as follows.

First, we examined three thermodynamic issues: spicity, elasticity and cabbeling; both the spicity and elasticity can be used as convenient tools in the study of thermohaline circulation. In particular, elasticity is directly connected to the instability of meso-scale thermohaline perturbations on quasi-horizontal surfaces (such as potential density surfaces), and it may be used to diagnose the energetics of meso-scale thermohaline perturbations on isopycnal surfaces.

Second, we conceptually separate the isopycnal diffusion into two steps, stirring and subscale diffusion. We postulate that meso-scale thermohaline perturbations on potential density surfaces (or quasi-neutral surfaces) may grow with GPE released through isopycnal stirring and cabbeling.

This is a new kind of meso-scale instability. Although this instability may be linked to the well-known instabilities associated with double diffusion and the baroclinic instability; it is also quite different from these two well-known types of instability.

Double diffusion instability is directly linked to the different diffusivity of heat and salt in the ocean according to the specific temporal and spatial scales involved. Most studies related to double diffusion have been primarily confined to the dynamical processes in the vertical plane. On the other hand, the meso-scale thermohaline perturbations discussed here takes place primarily on the quasi-horizontal surfaces, such as the potential density surfaces.

Baroclinic instability has been widely studied. The classical definition of baroclinic instability is characterized by the flattening of isopycnal surfaces. On the other hand, the new type

Table 4. Sensitivity of GPE source and sink (GW) to the time of data smoothing for the case of isopycnal coordinates

Terms	Grids	Smooth times	Stirring		Cabbeling	
			Source	Sink	Source	Sink
Diffusion	1.0	0	37	−76	0	−89
		1	21	−56	0	−69
		2	16	−47	0	−60
	0.5	0	23	−44	0	−55
		1	10	−32	0	−37
		2	6	−25	0	−29
Advection	1.0	0	339	−337	28	−22
		1	189	−207	12	−10
		2	134	−155	8	−6
	0.5	0	374	−390	17	−15
		1	237	−258	10	−8
		2	141	−163	6	−5

Notes: GPE changes is due to isopycnal stirring & advection. K=1 000 m^2/s for 1° resolution, and K=500 m^2/s for 0.5° resolution. Analysis is based on 50-year mean SODA data of salinity, temperature and horizontal velocity.

of instability postulated in this study is critically dependent on the nonlinear nature of the equation of state for seawater. Were the equation of state for seawater is linear, this new type of instability would not grow due to lack of mechanic energy for supporting. In addition, this new type of instability is linked to perturbations on potential density surfaces, so it does not require flattening of isopycnal surfaces. Of course, due to this type of instability and cabbeling associated mixing, new water mass can be formed and they can sink to the layer below. However, the details of this instability remain important dynamics issues for further study.

One of the most important issues we discussed in this study is the parameterization of quasi-horizontal diffusion of tracers in oceanic numerical models. A major point in this study is that quasi-horizontal diffusion should not be treated as homogeneous and isotropic; however, at this time, we do not really know the distribution of diffusivity in space and time. As a step forward, we have assumed a constant diffusivity and calculated the GPE balance of the world oceans; thus, the exact numbers cited in this study may not be what really appears in the ocean; nevertheless, these numbers may help us to understand something about quasi-horizontal diffusion in the ocean.

At this time, the total amount of mechanical energy available in the subsurface ocean for sustaining the oceanic wind-driven and thermohaline is on the order of 1 TW or less. Thus, the huge amount of GPE required to sustaining sigma surface diffusion or horizontal diffusion is not available in the ocean. Even the amount of mechanical energy required for sustaining isopycnal diffusion should be considered as a substantial portion of the total energy available. From the need of balancing the mechanical energy, hence, we conclude that the parameterization of sigma surface diffusion and horizontal diffusion, as commonly used in numerical simulations and discussed above, is unphysical.

In particular, although sigma coordinate models have been widely used in atmospheric and oceanic simulations, the huge amount of GPE required for sustaining such sigma surface stirring and cabbeling raises an important issue whether such lateral diffusion really happens in the ocean. This may be seen as a challenge to the numerical community to deal with the energetics of sigma coordinates model and the associated along-sigma-surface lateral diffusion.

In addition, our calculations indicate that lateral diffusion is not uniform or isotropic. Thus, the parameterization of lateral diffusion should be reexamined carefully. It is postulated that further study in parameterization of quasi-horizontal diffusion should take into consideration of mechanical energy balance, in particular the balance of gravitational potential energy.

The second issue discussed in this study is the artificial diffusion associated with the advection terms in Eulerian coordinates. With the advance of computer technique, many models are now running with horizontal resolution on the order of 1–10 km. The corresponding lateral eddy diffusivity is often set to rather small values or even zero. These numerical simulations are often called eddy-resolving simulations. However, our analysis in this study indicates that there is large numerical diffusion associated with the advection terms in the Eulerian coordinates. Thus, setting the lateral eddy diffusivity to zero does not mean there is no lateral eddy diffusion in the model. In fact, all it means is that lateral eddy diffusion in the model is out of our control. Solutions obtained from such simulation are heavily relied on the numerical diffusion generated by the horizontal advection terms. Since the lateral diffusivity is explicitly set to zero, there is no GPE release directly linked to stirring and cabbeling associated with lateral diffusion. It is important to understand the energetics of lateral diffusion in such model runs.

For a long time sigma coordinates model has been used to simulate coastal circulation, and recently these models are also being used for simulate circulation in a whole basin, including the deep part of the ocean. The fact that model based on sigma coordinates cannot simulate the eddy diffusion accurately is well known. Thus, the option of rotating the mixing tensor is also currently available in some sigma coordinate models. Although rotating the mixing tensor and use small eddy diffusivity may reduce the artificial eddy diffusion, the large artificial diffusion associated with the Eulerian coordinates remains a great challenge for sigma coordinates models.

A final remark is about the energetics formulae postulated in this study. Since our focused is on grid with horizontal resolution on the order of 1–100 km and vertical resolution on the order of tens of meters, our calculation is a calculation for turbulent motions. Within the whole paper, GPE source and sink is presented as the summary of horizontal contributions from 4 lateral sides for each (i, j, k) grid point. This is essentially equiv-

alent to assume that turbulent motions from all four sides of each grid point is statistically correlated.

From the theoretical point of view, of course, there is no reason to assume that turbulent motions in the vicinity of each grid point on such a relatively larger scale are synchronized. Thus, a possible alternative approach is to treat eddy diffusion from all four side boundaries of each grid point as independent, and the corresponding source and sink terms are summed up. It is clear that if such an assumption is made, the corresponding sum of source and sink would much increased. To limit the length of this long document, the details of such a calculation is, however, left for further study.

We have calculated many terms of GPE source and sink, and we postulate that these terms can be used as criteria for evaluate the performance of lateral diffusion and advection. At this time, it is not clear the exact criterion acceptable for ocean modeling; however, the following values may serve as the target upper limit: For lateral eddy diffusion, the GPE source and sink associated with stirring should be less than 0.1 TW; the GPE sink associated with cabbeling should be less than 0.1 TW.

For the lateral advection, it is not clear how to use the GPE source and sink due to stirring associated with advection. However, GPE source and sink due to cabbeling might be a useful criterion. Specifically, the sink should be limited to 0.1 TW, and the source is completely non-physical, and we recommend using zero as the target limit.

Over the past, many numerical models have been developed and used for global scale simulation of the oceanic general circulation. The formulations of these models are dramatically different in many fundamental aspects, such as the vertical and horizontal coordinates used in the models, the discretization of the primitive equations (different finite difference scheme, or different finite volume schemes), and the parameterization of the subscale processes. Hence the performance of these models is difficult to be compared.

One obvious way of model comparison is, of course, how well do outputs of these model match observations. However, model circulation involves complicated dynamical processes in space and time; as a result, such comparison cannot provide simple conclusion.

The crux of this study is to quantify the performance of the models in terms of GPE balance. Specifically, the focus is on the simulation of lateral diffusion and advection in the models. We formulated the GPE source and sink due to stirring and cabbeling associated with lateral diffusion and advection for Eulerian models based on three vertical coordinates.

Overall, the isopycnal coordinates provide the best performance among three coordinates. The advantage of isopycnal coordinates vs the z-coordinates is well-known in the numerical community; our study provides a qualitative and conclusive support.

Although sigma coordinate models have been widely used in the community as well, some of the fundamental issues related to this coordinate have not been thoroughly examined. In this study, we showed that the GPE source and sink in sigma coordinates is huge, about 1 000 time larger than the upper bound we postulated. In addition, we demonstrated that there are apparently major problems associated with sigma advection. The physical nature of such problems is also explored in details.

Our study posted major challenges for the model community. First, the application of sigma coordinate models for the open ocean circulation may be questionable. Second, the Eulerian coordinated models may produce large numerical errors associated with the lateral advection terms. Therefore, it is desirable to develop a new coordinate which can overcome such problems.

Acknowledgements

This study took more than three years to finish. During this long period of difficulty I received persistent encouragement from many of my colleagues. In particular, Quanan Zheng provided the most need support and suggestions, and I would take this opportunity to thank all my colleagues who gave the most needed support.

References

Carton J A, Giese B S. 2008. A reanalysis of ocean climate using simple ocean data assimilation (SODA). Mon Weather Rev, 136: 2999–3017

Huang R X. 2014a. Energetics of lateral eddy diffusion and advection: Part I. Thermodynamics and energetics of vertical eddy diffusion. Acta Oceanol Sin, 33(3): 1–18

Huang R X. 2014b. Energetics of lateral eddy diffusion and advection: Part II. Numerical diffusion/diffusivity and gravitational potential energy change due to isopycnal diffusion. Acta Oceanol Sin, 33(3): 19–39

Huang R X. 2014c. Energetics of lateral eddy diffusion/advection: Part III. Energetics of horizontal and isopycnal diffusion/advection. Acta Oceanol Sin, 33(3): 40–57

Appendix. Why GPE source due to sigma diffusion is so large

The GPE source and sink due to stirring and cabbeling along sigma surfaces is much larger than that associated with horizontal diffusion or isopycnal diffusion. This must be linked to the special way of handling lateral diffusion in the sigma models. We argue that the largeness of source and sink associated with sigma diffusion is due to the fact that in sigma models, warm water parcels from shallow levels is assumed to be mixed with cold water parcel from deeper levels. Mixing water parcels with such a large difference in properties can leads to big change in density and thus strong source and sink of GPE.

As an example, we demonstrate the large GPE source associated with sigma-surface stirring related to steep topography. For simplicity, we will use a simple one-dimensional periodic topography with valleys and seamounts lining up one next to another, as shown in Fig. A1. The pressure grid over the valley stations is taken as the standard pressure grid for the commonly used climatological datasets, such as WOA01 and WOA09, i.e. the center of the bottom grid in the valley is at 5 500 (10^4 Pa), with the corresponding sea floor at 5 750 (10^4 Pa). Thus, the centers of grid box in the vertical direction at the valley station are at 0, 10, 20, 30, 50, 75, 100, 125, 150, 200, 250, 300, 400, 500, 600, 700, 800, 900, 1 000, 1 100, 1 200, 1 300, 1 400, 1 500, 1 750, 2 000, 2 500, 3 000, 3 500, 4 000, 4 500, 5 000, 5 500 (10^4 Pa).

The station over the top of the seamount has the sea floor at 3 500(10^4 Pa), and the center of the bottom grid is at 3 341 (10^4 Pa). The rest of the pressure grid at the seamount stations is arranged according to the convention of the sigma coordinate model, as shown in Fig. A1. The center of each sigma grid box is marked by a black dot, and the lateral boundaries of the grid boxes are marked by red lines.

As the common practice, lateral diffusion in this coordinates is parameterized as sigma surface diffusion, i.e., it is assumed to be taken place along sigma surfaces, as schematically shown by the red arrows in Fig. A1. Note that such stirring forces water mass from quite different depth to exchange their position and mix. This is in a great contrast to the exchange of water masses along nearly horizontal surfaces, as indicted by the blue arrows in Fig. A1.

Assume that water property is homogeneous on pressure surfaces, and it varies with pressure only, i.e., potential temperature is an exponential function of pressure

$$\Theta = \Theta_0 \mathrm{e}^{-3p/p_\mathrm{b}} \tag{A1}$$

where Θ_0=25°C is potential temperature at the sea surface, p_b=5 500 (10^4 Pa) is the pressure at the center of the bottom grid, and salinity is set to be a constant value of 35 (Fig. A2).

Since salinity is assumed to be constant and potential temperature is a function of pressure only, isopycnal surfaces are coincident with pressure surfaces. Thus, both isopycnal stirring and horizontal stirring should take place in the directions indicated by the blue arrows in Fig. A1. Incidentally, there are no salinity and potential gradients in the horizontal direction, so that stirring along the horizontal direction does not produce any change in the system. However, stirring along the sigma surfaces should produce dramatic change of the temperature distribution and thus GPE of the system, as will be shown shortly.

First, we note that there is a large difference in potential temperature along sigma surfaces. Although temperature has a smooth profile in the ordinary pressure coordinate, it appears not so smooth when it is plotted in terms of the sigma layers, Fig. A3a; this is due to the fact that the thickness of the layers is discreet. The corresponding properties for a case with the top of seamount located at the pressure level of 3 000 (10^4 Pa) are shown in Fig. A3. Note that at the same sigma level, potential temperature difference can be quite large. For example, in the lowest layer, potential temperature difference is about 3.6°C. This large gradient of potential temperature on sigma surfaces is due to the fact that between two adjacent grid points sigma surfaces move over a great depth (pressure) range.

This fact has been hailed as a big advantage of sigma coor-

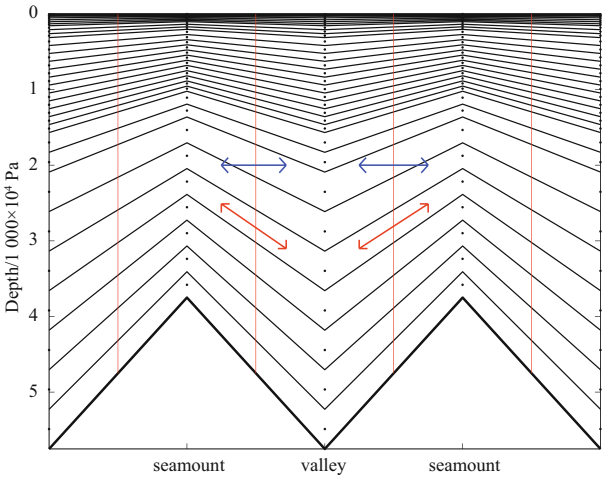

Fig.A1. A sketch of the pressure-sigma grid for an idealized one-dimensional periodic topography with valleys and seamounts. Red arrows indicate cross-grid boundaries diffusion along sigma surfaces and blue arrows indicate horizontal diffusion.

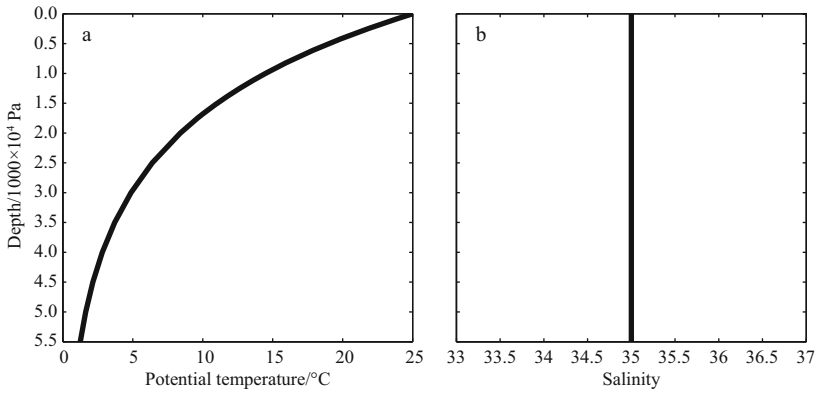

Fig.A2. Vertical profiles of potential temperature (a) and salinity (b) at a station over the valley. Variables are plotted in the pressure coordinate.

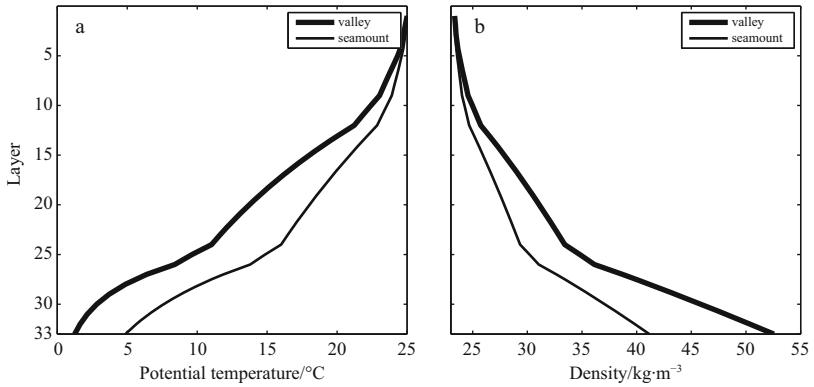

Fig.A3. Vertical profiles of potential temperature over valley and seamount (with the peak at 3 000 (10^4 Pa)) (a); density profile over valley and seamount (b). All variables are plotted in terms of layers in the sigma coordinate.

dinate models because they are able to deal with rough bottom topography. However, the ability of encompassing a large depth change of the sigma coordinate model is not without a price. One of the old issues in sigma coordinate models is the pressure gradient errors associated with steep topography. There is another potentially more critical issue related to the energetics of sigma surface diffusion. As shown in Fig. A1, sigma surface stirring and subscale diffusion imply exchanging and mixing of water masses taken over a quite large depth range, and these water masses can have quite large difference in their temperature and salinity.

In the present case, sigma diffusion implies bring water from 5 500 (10^4 Pa) and mixing it with water on the top of the seamount which is located at 3 000(10^4 Pa). Although simulating diffusion in sigma coordinates numerical model has been practiced many times over the past, nobody ever asked a nature question: is such a diffusion a realistic parameterization of the meso-scale eddies and turbulence in the ocean? In another word, are there really meso-scale motions in the ocean take place along such sigma surfaces?

For the case discussed here, Eq. (2) is reduced to

$$\dot{\chi}_{\text{stir}}^{\text{sigma,diffu}} = CK\Delta h P_{\text{fact}},\ P_{\text{fact}} = p\left(2 - \frac{\sigma_{i+1,k} + \sigma_{i-1,k}}{\rho_{i,k}}\right), \qquad \text{(A2)}$$

where p is the pressure at each grid point, $\sigma_{i-1,k}$ and $\sigma_{i+1,k}$ is the potential density of water parcels from the grid boxes on the right-hand side and the left-hand side. P_{fact} has the same dimension as the pressure, and it will be called the GPE factor; this factor can be used to evaluate the GPE source and sink, without specifying the diffusivity. Using Eq. (A2), the corresponding GPE source and sink associated with the valley stations and the seamount stations can be calculated.

Potential temperature over the top of the seamount is higher than that over the bottom of the valley. Thus, when a water parcel from the top of seamount arrives at the bottom of the valley, it should have an *in-situ* density lighter than the *in-situ* density of the water parcel originally sitting in the valley. As a result, there is a GPE source due to sigma surface stirring over the valley. Similarly, there should be GPE sink over the seamount. In the present case, the reason of the net GPE source due to stirring associated with sigma diffusion is clear. For grid points in the valley, sigma diffusion brings warm water from the top of the seamount; as a result, temperature in the valley increases. On the other hand, for grid points on the top of the seamount, the situation is opposite. Sigma diffusion brings in cold water from the valley and thus reduces the temperature at the top of the seamount. Therefore, the combination of sigma diffusion on the top of the seamount and in the valley gives rise to an

equivalent of warming and the abyss and cooling at the middle depth. This is equivalent to the effect of vertical diffusion, which leads to the increase of GPE.

Since pressure at the valley station on the corresponding sigma surfaces is much larger than that at the seamount station, the absolute value of GPE source associated with sigma stirring at the valley station is much larger than the absolute value of the GPE sink at the seamount station. Both the strength of source and sink increases with pressure, except for the last four layers, Fig. A4a. As a result, the vertically accumulated source and sink increases rapidly with pressure, and the total amount of source are about more than twice as that of the sink (Fig. A4b).

In general, the ratio of the absolute value of source and sink rapidly increases with the increase of the seamount height (or the reduction of the distance between the sea surface and the top of the seamount) (Fig. A5). Our discussion here gives a theoretical explanation for the large difference in the absolute value of GPE source (123.8 TW) to the GPE sink (48.9 TW) diagnosed from the SODA data as presented above.

A close examination of the temperature difference and the amount of GPE source and sink associated with sigma stirring and mixing discussed above suggested that such motions across a large depth range may not really happen in the ocean. Since there are no such huge amount of mechanical energy available in the ocean, sigma surface stirring and subscale diffusion implicitly postulated in basin-scale models based on sigma coordinates cannot be supported by the fundamental physics of the oceanic circulation.

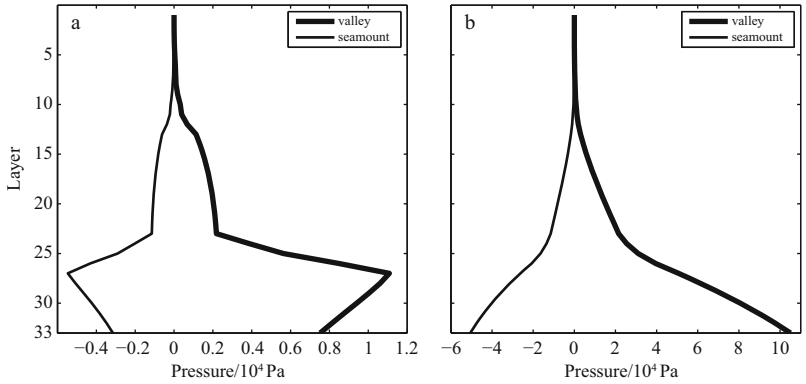

Fig.A4. Vertical distribution of GPE factor due to stirring associated with sigma diffusion: local source and sink (a), vertical accumulation (b).

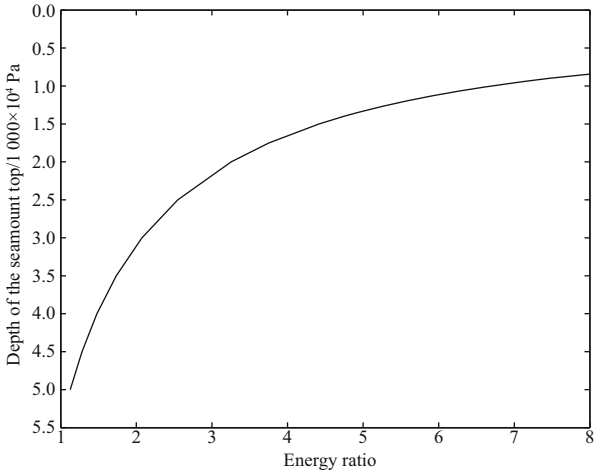

Fig.A5. Ratio of GPE source and sink as a function of the seamount depth (the valley is at the depth of 5 500 (10^4 Pa)).